TAMPERE UNIVERSITY OF TECHNOLOGY

SUVI LEHTIMÄKI

ION GELS AS GATE DIELECTRICS IN ORGANIC THIN-FILM TRANSISTORS

Master of Science Thesis

Examiners:
Professor Donald Lupo
Professor Helge Lemmetyinen
Examiners and topic approved in the
Science and Environmental
Engineering Faculty Meeting
December 12th, 2011

ABSTRACT

TAMPERE UNIVERSITY OF TECHNOLOGY
Master's Degree Programme in Science and Technology
SUVI LEHTIMÄKI: Ion gels as gate dielectrics in organic thin-film transistors
Master of Science Thesis, 56 pages
February 2012
Major: Chemistry
Examiners: Donald Lupo, Helge Lemmetyinen
Keywords: organic electronics, organic thin-film transistor, ion gel, ionic liquid

Ion gels composed of ionic liquids and block copolymers can be used as gate dielectrics in organic thin-film transistors. Conventional dielectrics used in OTFTs do not have capacitances large enough to enable transistor operation at low voltages, which is needed in many organic electronics applications. Mobile ions in the gel form electric double layers, giving rise to a very high capacitance and therefore high charge carrier concentrations at low operating voltages.

The goal of this study was to fabricate a functioning OTFT using an ion gel as gate dielectric, and to examine its properties. The OTFT was prepared with a top-gate geometry, where the ion gel was sandwiched between the gate electrode and the substrate with the semiconductor channel. The semiconductor was amorphous poly(triarylamine), which was deposited by spin-coating. The ion gel gated OTFT properties were compared with a reference OTFT structure, which had a conventional polymeric gate dielectric.

The ion gel gated transistor operated with voltages below 2 V and the output current was three orders of magnitude larger than that of the reference OTFT, which required more than ten times the voltage. The capacitance of the ion gel was over 5 $\mu F/cm^2$ up to 1 MHz. The charge carrier mobility in the OTFT was on the order of $10^{-3}\,cm^2/(Vs)$, which was similar to that in previous studies with the semiconductor used. The transistor could be switched on and off at the frequency of 1 kHz, but there was a large overlap capacitance across the gel.

Hysteresis and leakage were challenges in the ion gel gated OTFT preparation. The ionic liquid is hygroscopic, making the gel susceptible to water impurities. The impurities can cause leakage and hysteresis due to electrochemical reactions at the electrodes even at low voltages. Future work with ion gel gated OTFTs will require a more controlled environment in terms of ambient humidity.

TIIVISTELMÄ

TAMPEREEN TEKNILLINEN YLIOPISTO
Teknis-luonnontieteellinen koulutusohjelma
SUVI LEHTIMÄKI: Ion gels as gate dielectrics in organic thin-film transistors
Diplomityö, 56 sivua
Helmikuu 2012
Pääaine: kemia
Tarkastajat: Donald Lupo, Helge Lemmetyinen
Avainsanat: orgaaninen elektroniikka, orgaaninen ohutkalvotransistori, ionigeeli, ioninen neste

Ionisista nesteistä ja kopolymeereistä koostuvia ionigeelejä voi käyttää hilaeristeinä orgaanisisssa ohutkalvotransistoreissa. Perinteisesti orgaanisissa transistoreissa käytetyillä eristeillä ei ole riittävän suurta kapasitanssia, jotta transistori toimisi matalilla jännitteillä. Monet orgaanisen elektroniikan sovellukset vaativat matalia jännitteitä. Ionigeelin sisältämät ionit muodostavat sähköisen kaksoiskerroksen, joka aiheuttaa suuren kapasitanssin ja saa siten aikaan suuren varaustiheyden jo pienellä jännitteellä.

Tämän tutkimuksen tavoitteena oli valmistaa toimiva orgaaninen ohutkalvotransistori käyttäen ionigeeliä eristeenä, sekä tutkia transistorin ominaisuuksia. Transistori valmistettiin levittämällä ionigeeli puolijohdekanavan päälle ja asettamalla hilaelektrodi sen päälle. Puolijohteena käytettiin poly(triaryyliamiinia), joka levitettiin spinnipäällystysmenetelmällä. Ionigeelitransistorin ominaisuuksia verrattiin transistoriin, jossa käytettiin eristeenä tavanomaista polymeerimateriaalia.

Ionigeelitransistori toimi alle 2 V:n jännitteillä. Sen ulostulovirta oli kolme kertaluokkaa suurempi kuin vertailutransistorin, joka vaati yli kymmenen kertaa suuremman jännitteen toimiakseen. Ionigeelin kapasitanssi oli 5 $\mu F/cm^2$ alle 1 MHz:n taajuuksilla. Varaustenkuljettajien liikkuvuudeksi määritettiin noin 10^{-3} $cm^2/(Vs)$, mikä on samaa suuruusluokkaa kuin aiemmat tulokset samalla puolijohdemateriaalilla. Transistorin kytkeminen päälle ja pois onnistui taajuudella 1 kHz, mutta transistorissa oli suuri ylimääräinen kapasitanssi johtuen hilaelektrodin päällekkäisyydestä muiden elektrodien kanssa.

Ionigeelitransistorin valmistuksessa haastavia olivat hystereesi ja vuotovirta ionigeelin läpi. Käytetty ioninen neste on hygroskooppista, minkä vuoksi geeli oli altis ympäristön vedelle. Vesi ja muut epäpuhtaudet aiheuttavat hystereesiä ja vuotoa, koska ne voivat reagoida sähkökemiallisesti elektrodeilla jo pienillä jännitteillä. Tulevaisuudessa ionigeelitransistorien kehittäminen vaatii hallitummat olosuhteet, jotta ilman vesihöyry ei pääse kosketuksiin geelin kanssa.

PREFACE

The work for this thesis was carried out in the Organic Electronics group at the Department of Electronics at Tampere University of Technology. The work was done during the summer and fall of 2011 as a part of the PETRA project funded by UPM-Kymmene Corporation.

I wish to thank my examiner Prof. Donald Lupo for the position as a research assistant in his group and for his advice in my work. I thank my examiner Prof. Helge Lemmetyinen for advice during the writing and for the valuable experience I gained as a summer worker at the Department of Chemistry. I wish to thank M.Sc. Marika Janka for her guidance in the practical work and in the writing of this thesis. I also thank her for preparing the evaporated substrates for my samples.

I thank M.Sc. Petri Heljo for his advice, especially with electrical measurements. I give my thanks also to the rest of the group for the good working environment: Sampo, Kaisa, Miao and Santtu, and especially Tuomas for the many helpful and pleasant conversations.

I thank my parents for supporting me in my studies for all these years. Finally, I thank Jouni for his love and support.

Tampere, January 9th, 2012

Suvi Lehtimäki

CONTENTS

ABBREVIATIONS

AMOLED	active-matrix organic light-emitting diode display
a-Si	amorphous silicon
BJT	bipolar junction transistor
$BMIPF_6$	1-butyl-3-methylimidazolium hexafluorophosphate
CMOS	complementary metal-oxide-semiconductor
D	drain electrode
DC	direct current
DE	dielectric
DOS	density of states
EMITFSI	1-ethyl-3-methylimidazolium bis(trifluorosulfonyl)amine
$EMIOctOSO_3$	ethylmethylimidazolium *n*-octylsulfate
EtAc	ethyl acetate
F8T2	poly(9,9-dioctylfluorene-*co*-bithiophene)
FET	field-effect transistor
G	gate electrode
HOMO	highest occupied molecular orbital
ITO	indium tin oxide
LUMO	lowest unoccupied molecular orbital
MISFET	metal-insulator-semiconductor field-effect transistor
MOS	metal-oxide-semiconductor
MOSFET	metal-oxide-semiconductor field-effect transistor
OFET	organic field-effect transistor
OTFT	organic thin-film transistor
P3HT	poly(3-hexylthiophene)
PEDOT:PSS	poly(3,4-ethylene dioxythiophene):poly(styrenesulfonate)
PET	poly(ethylene terephtalate)
PMMA	poly(methyl methacrylate)
PQT-12	poly(3,3"'-didodecylquaterthiophene)
PS	polystyrene
PTAA	poly(triarylamine)
PVP	poly(4-vinylphenol)
RFID	radio-frequency identification
S	source electrode
SAM	self-assembled monolayer
SC	semiconductor
SMS	polystyrene-*b*-poly(methyl methacrylate)-*b*-polystyrene
TFT	thin-film transistor

SYMBOLS

A	area
C	capacitance
C_i	specific capacitance
d	insulator thickness
E_C	conduction band edge energy
E_F	Fermi energy
E_i	intrinsic Fermi energy
E_V	valence band edge energy
E_vac	vacuum energy level
ϵ_r	relative permittivity
ϵ_0	vacuum permittivity
Φ	work function
Φ_F	Fermi level and intrinsic Fermi level difference
g_m	transconductance
I_D	drain current
$I_{D,lin}$	drain current in the linear region
$I_{D,sat}$	drain current in the saturation region
k	relative permittivity
L	channel length
μ	charge carrier mobility
N_a	acceptor dopant concentration
q	unit charge
R	resistance
S	subthreshold slope
τ	time constant of an RC circuit
V_D	drain voltage
V_{FB}	flat-band voltage
V_G	gate voltage
V_T	threshold voltage
W	channel width

1 INTRODUCTION

Organic electronics is a rapidly growing interdisciplinary field. Its beginning was the discovery of conductive polymers by Heeger, MacDiarmid and Shirakawa et al. in 1977 [1], for which they were awarded the Nobel Prize in Chemistry in 2000 [2]. The advantages of organic electronic devices compared to traditional inorganic electronics lie in their low cost and facile deposition by e.g. printing. Organic electronics materials also offer endless possibilities for tuning their properties by changes in chemical structure. Although organic devices cannot replace inorganic-based ones in most applications, they open up new possibilities for flexible and large-area electronics. Interesting organic electronics devices include light-emitting diodes [3], solar cells [4], diodes [5, 6] and thin-film transistors [7], the last of which is the subject of this work.

Organic thin-film transistors (OTFT) have the same basic structure as inorganic thin-film transistors used commonly in displays. The defining characteristic of OTFTs is that the active layer, semiconductor, is an organic material; it is either a polymer or a small organic molecule. The electrodes and the insulator layer may be organic or inorganic. Prospective applications for OTFTs include active matrix displays [8–10], RFID tags [11], and sensors [12, 13].

In many applications for OTFTs, low voltages are desired. The output voltage of thin-film batteries is usually only 1–2 V [14]. External RF-fields or energy-harvesting devices, such as solar cells, also generally produce only small voltages [14]. Unfortunately, OTFTs usually require high voltages of over 20 V. This is mainly because the charge carrier mobilities of organic semiconductors are low, requiring a high dielectric layer capacitance to accumulate enough charge carriers. The capacitances are usually low, since the layers have to be made thick in order to avoid leakage current through it, and because the dielectric constants are low [15].

Efforts to increase the dielectric layer capacitance include using high-dielectric constant insulators [16] or achieving an ultrathin dielectric with self-assembled monolayers [15]. An interesting approach is using a dielectric containing mobile ions. The ions form electric double layers at the gate electrode and semiconductor surface, decreasing the effective thickness of the dielectric to molecular dimensions and facilitating a large charge carrier concentration to accumulate to the semiconductor. The different methods for utilizing ion-based gate dielectrics include an anionic

polymer [17], ion-conducting membrane [18] and the type examined in this thesis, an ion-containing gel [19].

Ion gels used as gate dielectrics were introduced by the Frisbie group [20]. The gels consist of an ionic liquid and a block copolymer, which form a physically cross-linked gel. An ionic liquid is an organic salt which is liquid at room temperature. The ions of the liquid are able to move inside the gel, enabling the formation of the electric double layers. A transistor based on an ion gel can be operated at voltages below 2 V. These transistors do have some drawbacks, such as slow switching due to the limiting ion mobility in the gel, and leakage through the insulator caused by electrochemical reactions.

The objective of the work done for this thesis was to study the structure and properties of ion gel gated organic thin-film transistors and to fabricate an ion gel gated transistor that could function at low voltages. Such a transistor is needed to function in a circuit with printed organic diodes [5], which cannot withstand the high voltages the conventional OTFTs require. Chapter 2 reviews the theoretical background for the thesis. This includes the nature of charge conduction in organic semiconductors and the operating principle of field-effect and thin-film transistors, as well as the properties of ionic liquids and ion gels. The experimental details are presented in Chapter 3, and the results are discussed in Chapter 4.

2 THEORETICAL BACKGROUND

2.1 Organic semiconductors

Organic materials that have semiconducting or conducting properties are essential to the field of organic, flexible and printed electronics. Their structure is very different from inorganic semiconductors, which consist of a closely spaced and highly ordered lattice of atoms. Organic semiconductors are molecular or polymeric materials, which are held together mainly by weak van der Waals forces.

Conducting polymers have a variety of different structures, but they all have one thing in common: a conjugation of alternating double and single bonds along the polymer backbone. This is why the terms *conjugated* and *conducting* are often used synonymously when dealing with polymers [21]. Small conjugated organic molecules such as pentacene and rubrene are also semiconducting and have been widely studied as materials in organic electronics [22]. This work will however focus on polymeric materials.

2.1.1 The molecular structure of organic semiconductors

According to the Hückel model, covalent double bonds between carbon atoms arise when the atoms are sp^2-hybridized with one valence electron in a non-hybridized p-orbital. The hybridized orbitals form σ bonds with neighboring atoms. The p-orbitals are perpendicular to the plane of the hybridized orbitals and form a π bond (π molecular orbital) between two carbon atoms. The π bond extends both above and below the molecular axis as depicted in Fig. 2.1(a). To obtain a bonding π orbital, the p orbitals must be combined symmetrically, i.e. the signs of the wave functions must match. When the p orbitals are combined antisymmetrically, the result is an antibonding π^* orbital, which has a higher energy. Each orbital can hold two electrons with opposite spins. [23, p. 563–564]

Alternating single and double bonds in a carbon chain correspond to non-hybridized p orbitals on each carbon atom, each orbital perpendicular to the plane of the zigzagging carbon chain. These p orbitals together form π molecular orbitals that extend the length of the chain, which means the electrons in these orbitals are delocalized. These are depicted in Fig. 2.1(b) for butadiene. The number of π molecular orbitals formed is the same as the number of p orbitals taking part in the

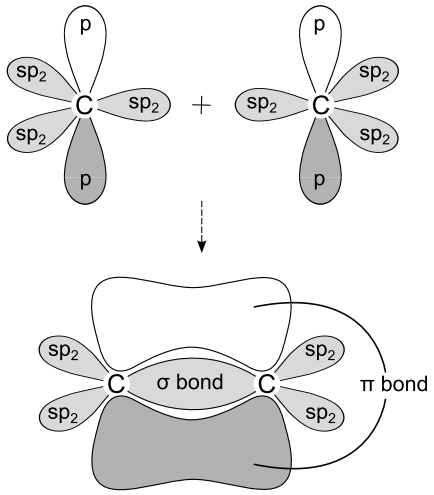

(a) The formation of double bonds.

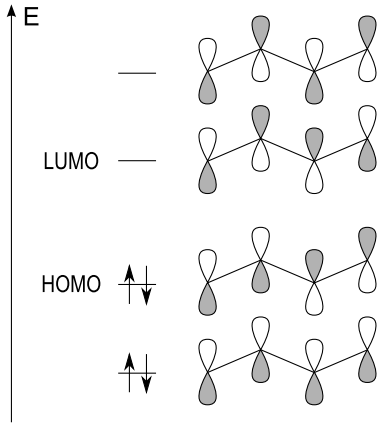

(b) The different combinations of p orbitals in butadiene [23].

Figure 2.1. *Conjugation arises from non-hybridized p orbitals. Each orbital originally holds one electron. The dark and white lobes of the p orbitals denote different signs of the wave functions.*

conjugation. The electrons occupy the lowest possible energy levels, giving rise to the highest occupied (HOMO) and lowest unoccupied (LUMO) levels. As the chain length grows, the energy levels become more closely spaced [24]. This is depicted in Fig. 2.2 for polyenes, the simplest conjugated molecules. Polyacetylene was the first conjugated polymer to be observed having electrical conductivity [1].

In polyacetylene, a phenomenon called the Peierls instability causes the structure to dimerize: the bonds between the carbon atoms in the chain are not equally

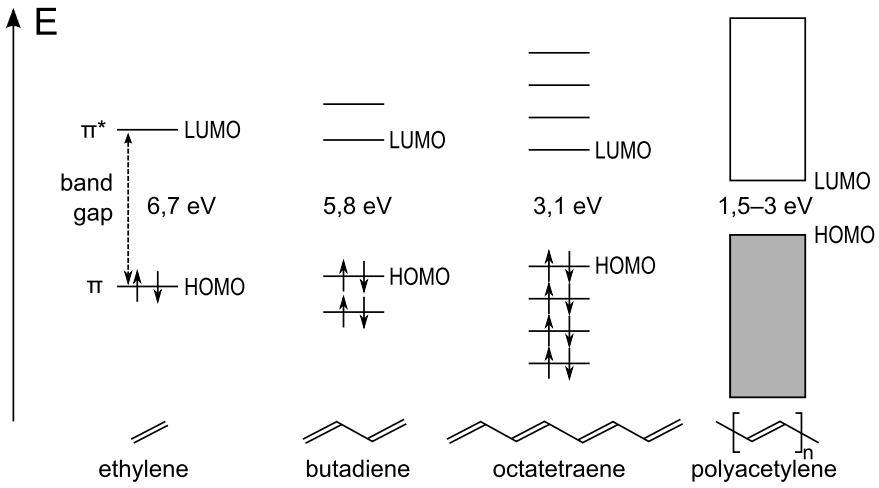

Figure 2.2. *As the chain length grows with alternating single and double bonds, the HOMO energy moves higher and the band gap decreases. Adapted from [25].*

spaced, but the distance alternates between shorter and longer. The dimerization is energetically more favorable than equal bond lengths. Because of the Peierls instability, there is a band gap even in an arbitrarily long polyacetylene molecule. [2, 26]

The average length that the π molecular orbitals extend is called the conjugation length. As can be seen from Fig. 2.2, the difference in the energy between the HOMO and LUMO levels (the band gap) decreases as the conjugation length increases. The same conclusion can be drawn from the very simple quantum mechanical "particle in a box" problem, where the spacing of consecutive energy levels decreases as the box length increases [27, p. 256]. This also leads to colors: when the band gap is smaller than the energy of photons in the visible part of the spectrum, the molecule can absorb them, which raises one electron to a higher energy level. The HOMO level energy represents also the oxidation energy of the polymer: a higher HOMO level corresponds to a smaller oxidation potential, which means the polymer is more susceptible to oxidation [28]. This can be harmful in applications where oxidation destroys the sample.

The conjugation length is not defined by the chain length alone. Especially in amorphous polymers, there are interferences in the π conjugation due to the disordered structure of the polymer. It is affected by not only the polymer structure, but also the synthesis and processing history of the material. [24]

Some common conjugated polymers used in OFETs are depicted in Fig. 2.3. Partially crystalline poly(3-alkylthiophene)s are among the most extensively studied polymers in many organic electronics applications, due to their good processability. The most common example of these is poly(3-hexylthiophene) (P3HT). A problem

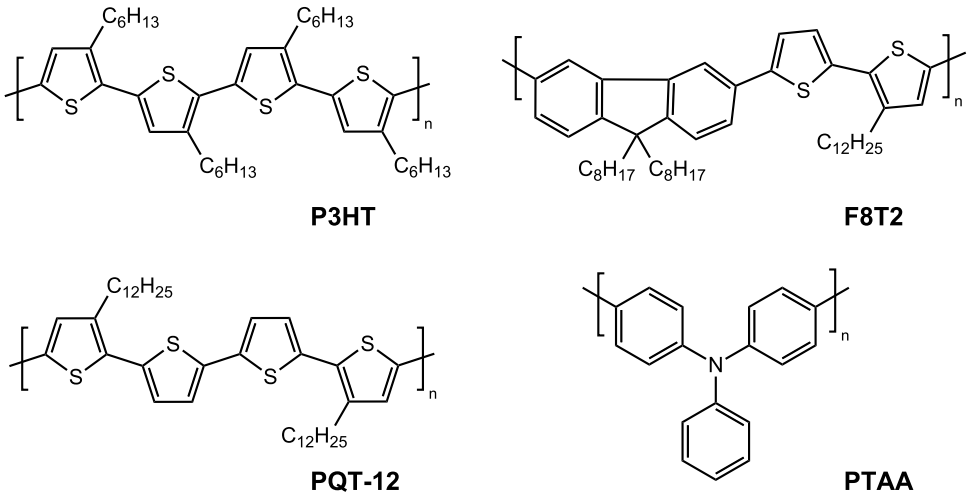

Figure 2.3. *Some common conducting polymers used in organic electronics applications: poly(3-hexylthiophene) (P3HT), poly(3,3"'didodecylquaterthiophene) (PQT-12), poly(9,9-dioctylfluorene-co-bithiophene) (F8T2) and poly(triarylamine) (PTAA) [22].*

for these polymers is the difficulty of synthesis of regioregular polymers[1] as well as their degradation in air. P3HTs generally have high conjugation lengths, which increases the HOMO energy, making the polymer more susceptible to oxidation. Stability issues have been addressed e.g. by changing the substituents (polyquaterthiophenes such as PQT-12) or by introducing fluorene moieties into the chain (F8T2). [22, 28]

Conducting polymers based on poly(triarylamine) (PTAA) are completely amorphous materials. They are generally highly soluble and don't require high-temperature annealing in the fabrication process. The amine nitrogen prevents efficient conjugation between the phenyl rings, which lowers the effective conjugation length. This in turn lowers the HOMO energy, improving the polymer's stability toward oxidation. There is however a trade-off: the disordered structure cannot offer as good charge transport properties as a crystalline material. PTAA is the polymer used in this work. [28]

2.1.2 Charge transport in organic semiconductors

In early research, conductivity could only be reached with chemical dopants such as halogen atoms, which oxidize the polymer. This creates a radical cation that can move along the chain. More recently, focus has shifted towards polymers where charge can be injected into the material from electrodes or to the electrodes from the material. This is important in applications such as field-effect transistors, light-emitting diodes and solar cells. [29]

When a charge is introduced into a polymer semiconductor, a radical cation or anion is formed. The charge also causes polarization in the surrounding polymer chain segments and other molecules: the electron distributions change to accommodate the new charge, with the atomic nuclei relaxing to a new configuration. The charge accompanied by the deformation around it is called a *polaron* [30]. When the charge is introduced by chemical doping with e.g. halogen atoms, the polarons are quite localized. This can easily be understood since the counter ion stabilizes the oppositely charged polaron. In the case of charge injection from electrodes, such as in the field-effect transistor, the polarons are spread over much larger distances. [31]

In some polymers, two polarons can bind together to form a *bipolaron* (Fig. 2.4), which is a more stable structure. If a molecule has a degenerate ground state (the lowest energy can be attained with different configurations), a *soliton* can form. Like polarons, soliton formation also causes bond distortion that spreads over many monomer units. Solitons can be neutral or charged. [32]

[1] Regioregular polymerization refers to polymerization where the monomer units are joined head-to-tail so that they have the same orientation in the chain.

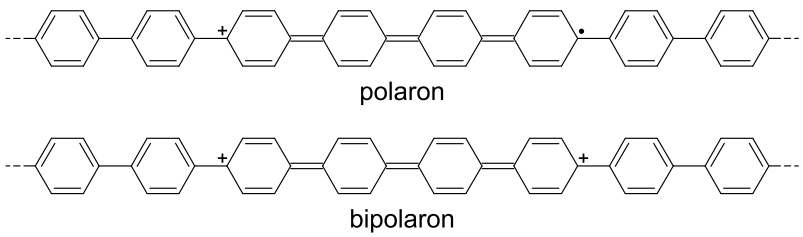

Figure 2.4. *A positively charged polaron and doubly positive bipolaron in poly(p-phenylene), spread out over four monomer units [24].*

There are many models for the charge transport in organic semiconductors, and the exact mechanism is not known exactly. In inorganic semiconductors, the periodic lattice structure allows for the wave functions of the individual atoms to overlap and form continuous energy bands, where charge carriers can move relatively freely [33]. In organic materials there is usually much disorder, which prevents band transport; polymeric semiconductors can even be completely amorphous. The disorder results in localization of the charges as polarons. [26]

The generally accepted model for charge transport in organic materials is the *hopping* model, which means a sequential redox process over molecular sites [30]. Hopping is thermally activated, which means that the conductivity increases with temperature; this is indeed observed in amorphous polymer semiconductors [34]. Charges can also tunnel between sites, but this type of transfer is dominant only at very low temperatures. At room temperature hopping is dominant [35]. The temperature dependence presents a clear difference to inorganic crystalline semiconductors, where the conductivity decreases with temperature due to increased lattice scattering of charge carriers [33].

The hopping process can be described by applying the *Marcus electron transfer theory* [36], which was originally derived for redox reactions in solution. The Marcus theory states that in order for the charge transfer to occur, the initial and final states must be distorted to a common configuration. It is useful in understanding the microscopic processes of charge transfer [34]. Simpler models have been derived to use with large, disordered systems [26, 37].

Organic semiconductors are usually divided into hole- (p) and electron- (n) transporting materials. This division is however very different from inorganic p- and n-type semiconductors, where the charge carrier type is determined by doping impurities. With organic semiconductors the classification is made simply by which type the material performs better with in devices. This in turn is mostly determined by the efficiency of charge injection at electrodes, and not by the actual mobility of the charge in the material. Generally, materials with high-lying HOMO levels are hole-transporting, and materials with low LUMO levels are electron-transporting.

There are also many compounds which are ambipolar, i.e. they can transport both electrons and holes well. [21, 35]

2.1.3 Contacts between a semiconductor and a metal

In devices, charges are usually injected into the semiconductor from a metal electrode. Thus it is important to understand the nature of the junction between a semiconductor and a metal. To get a basic picture of junction properties, inorganic semiconductor junctions with metals can be examined. Though the charge transport mechanisms differ, the principles of junction formation are the same for organic and inorganic semiconductors. Since most organic semiconductors, including the ones used in this work, are hole-transporting, p-type semiconductor junctions with metals will be examined.

When a metal and a semiconductor are brought into contact, there is a charge transfer across the junction in such a way that the Fermi levels of the materials align. This can result in a rectifying contact (Schottky contact), or a contact through which current can flow quite freely (ohmic contact). The contact type depends on the work functions of the materials: the work function Φ is the energy required to remove an electron from the surface. Since the Fermi level is the energy where the electron occupation probability is $\frac{1}{2}$, the work function is essentially the difference in energy between the Fermi level and the vacuum level (free electron energy). [33]

If the work function of the metal Φ_m is smaller than that of the p-type semiconductor Φ_s (the semiconductor Fermi level is lower), electrons will flow from the metal to the semiconductor valence band, which is at a lower energy. The metal is left with positive charges at the interface. At the semiconductor side of the interface a depletion region is formed, where acceptor dopant ions are not compensated by holes. The conduction and valence bands bend, giving rise to an energy barrier for holes in the junction, which is illustrated in Fig. 2.5. This is called the Schottky

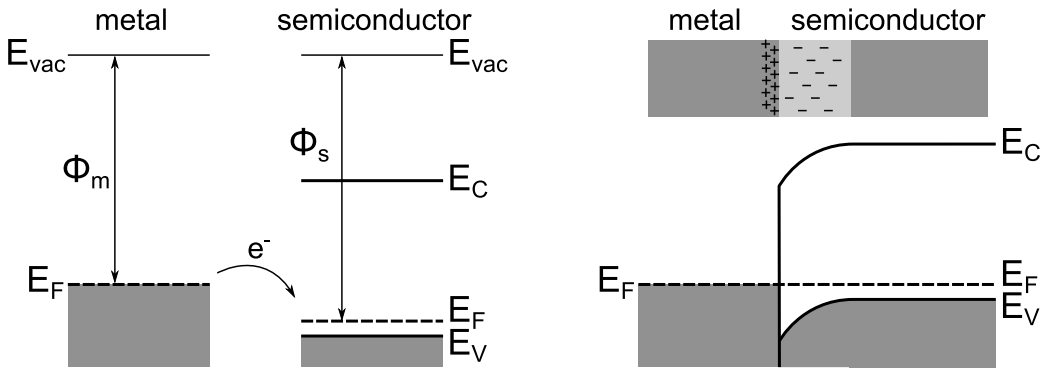

Figure 2.5. *A Schottky contact between a metal and a p-type semiconductor. Adapted from [33, p. 229].*

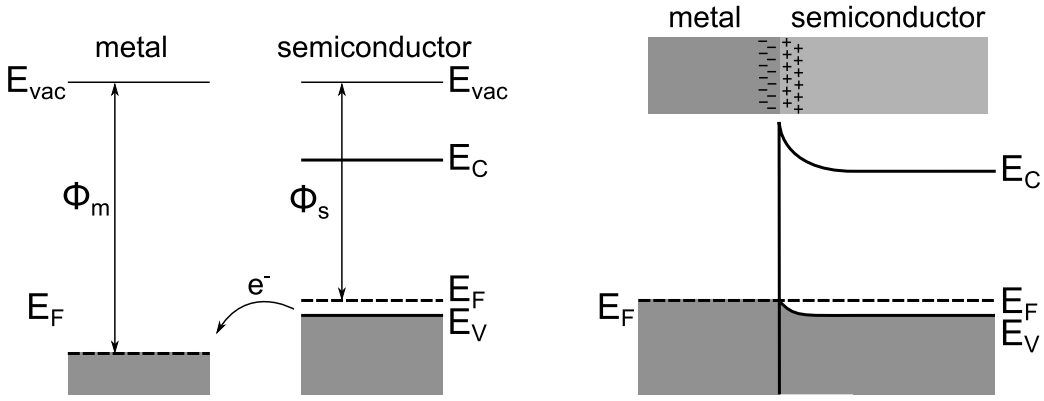

Figure 2.6. *An ohmic contact between a metal and a p-type semiconductor [33, p. 232].*

barrier. The barrier height can be reduced or increased by applying an external voltage. This results in rectification: in forward bias (semiconductor biased positively) the current flows quite freely, but in reverse bias it does not. [33, pp. 227–230]

When the work function of the metal is greater than the work function of the p-type semiconductor, the charge transfer of contact formation is in the other direction: holes accumulate at the semiconductor side of the junction and electrons in the metal side. The barrier (Fig. 2.6) to charge carrier flow through the junction is small and only a low external voltage is enough to overcome it. This is called an ohmic contact. [33, pp. 231–232]

In devices, ohmic contacts are desirable when efficient charge injection is needed. This is the case with e.g. field-effect transistors. The HOMO energy level of the organic semiconductor corresponds to the valence band of the inorganic semiconductor. Since the Fermi level of a p-type semiconductor is usually a little above the valence band, an ohmic contact requires that the metal Fermi level is approximately at the same energy as the semiconductor HOMO level or lower. This means that the metal work function should be equal to or greater than the semiconductor ionization energy.

The semiconducting polymer used in this work, PTAA, has a LUMO level at –1.8 eV and a HOMO level at –5.1 eV [38]. Gold, the electrode material used in this work, has a work function of 5.3–5.4 eV depending on crystal directions (measured from the photoelectric effect) [39]. This means that the Fermi level of gold is lower than the HOMO level of PTAA, which results in an ohmic contact between the two materials.

2.2 Field-effect transistors

Transistors are essential components in modern electronics. They are three-terminal devices where the input voltage or current of one terminal controls the current that

flows between the two other terminals. There are two basic types of transistors: the bipolar junction transistor (BJT) and the field-effect transistor (FET). The principle of the FET was proposed first by Lilienfield in 1930, whereas the first working transistor device was the BJT, which was invented by Bardeen, Brattain and Shockley in 1948. The first field-effect transistor was the metal-insulator-semiconductor FET or MISFET, and it was invented in 1960. The MISFET where the insulator is an oxide is referred to as MOSFET and it has taken its place as the most important type of transistor. Since many of the equations of MISFETs apply also to organic transistors, the properties of MISFETs are examined in this section. [33, pp. 251–252]

2.2.1 Operation of field-effect transistors

The field-effect transistor has three terminals: the *gate* (G), *source* (S) and *drain* (D) electrodes. The source terminal is usually connected to the ground and the other voltages are given relative to this. The voltage applied to the gate electrode controls the current between the source and drain electrodes when there is a supply voltage between the source and the drain. The term field-effect originates from the electric field induced by the gate, which controls the formation of a conducting semiconductor channel between the other two terminals. [33]

The basic operations of a FET are amplification and switching. Amplification means that a small variation in the input voltage, i.e. the gate voltage, induces a large variation in output currents between the source and the drain. Switching means that the device can be turned *on* and *off* by changing the gate voltage: the *off* state means that the current between the source and the drain is zero. Switching is generally used in digital circuits. [33]

The structure of a n^+-p-n^+ MISFET is shown in Fig. 2.7(a). The substrate in this case is a p-type semiconductor, and the source and drain connections are doped heavily n-type to get a good contact to the metal electrodes. When the device is on, there appears a conducting n-type channel between the source and the drain, and current can flow. The substrate can also be n-type, in which case the channel formed is p-type. The transistor function in the former case will be examined. The p-type channel is similar but the gate and drain voltages have opposite signs. [33, 40]

The energy bands of the MIS structure are shown in Fig. 2.7(b); the metal is the gate electrode. The vacuum level energy, E_{vac}, is the energy of a free electron. The conduction and valence band edges of the semiconductor are E_C and E_V, respectively. Approximately in the middle of the band gap lies the intrinsic Fermi level, E_i, which is the Fermi energy of the semiconductor when it is not doped. Ideally, the energy bands of the MIS capacitor are flat as in the figure, but in reality to achieve flat bands there has to be an applied external voltage to compensate the

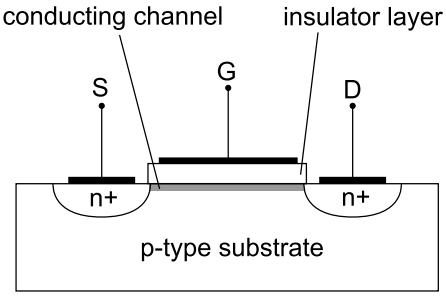

(a) The structure of a MISFET. The conducting n-type channel between the source and the drain is formed in the p-type semiconductor.

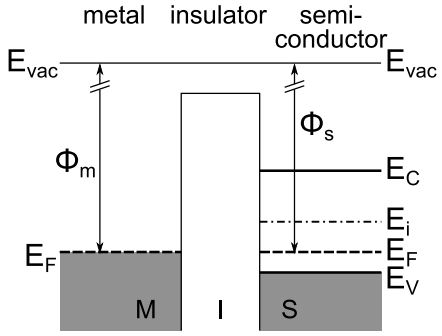

(b) The equilibrium energy bands in the ideal MIS structure.

Figure 2.7. *The structure and energy bands in a MISFET when the semiconductor is p-type. Adapted from [40].*

different work functions of the metal and the semiconductor. [33]

When a negative voltage is applied to the gate electrode, electrons accumulate on the metal side of the MIS capacitor. This in turn induces *hole accumulation* on the semiconductor side of the insulator. The semiconductor bands bend as depicted in Fig. 2.8(a). When a positive voltage is applied to the gate, the opposite happens: holes are *depleted* from the insulator interface (Fig. 2.8(b)). [33]

When a large enough positive voltage is applied to the metal, the semiconductor bands bend so much that the intrinsic Fermi level E_i crosses E_F. This results in *inversion*: a high population of electrons in the conduction band at the semiconductor-insulator interface (Fig. 2.8(c)). This can be understood in terms of n-type semiconductors, where the Fermi level is above E_i and there are electrons occupying the conduction band. Inversion creates a conducting channel between the source and drain electrodes, along the semiconductor-insulator surface and the device is turned on. [33, 40]

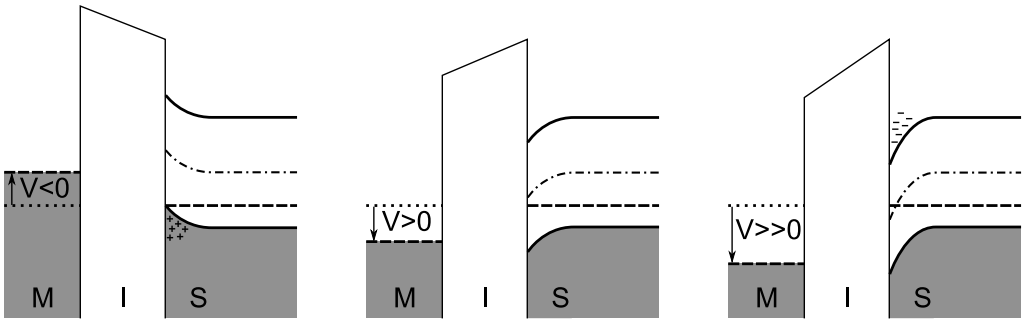

(a) Accumulation (b) Depletion (c) Inversion

Figure 2.8. *The effect of an applied voltage in the MIS structure. The energy levels are those presented in Fig. 2.7(b). Adapted from [40].*

Normal MISFET devices operate under inversion conditions. This is useful in manufacturing integrated circuits, because there are depletion regions between the rest of the substrate and the channel and the source and drain contacts. Other devices can be made on the same substrate, which facilitates easy integration of many MISFETs. [40]

The gate voltage at which strong inversion begins, is called the threshold voltage V_T. If the threshold voltage is negative, there is an inversion layer formed at zero gate voltage. In this case the device is referred to as a depletion-mode or 'normally on' device. There needs to be an applied voltage to turn the transistor off. The more common case is the enhancement-mode or 'normally off' mode, where there is no channel at equilibrium and the applied gate voltage induces it. [33, p. 267]

2.2.2 Output characteristics of MISFETs

Transistor output characteristics can be analyzed by applying a constant gate voltage V_G, sweeping the drain-source voltage, V_D, and measuring the drain current I_D. A representative set of output curves with different gate voltages is given in Fig. 2.9. Initially the current varies linearly with V_D, but after a certain voltage levels off to a saturation value. The saturation current is larger the more positive the gate voltage is. [33]

As the drain voltage increases, the voltage across the insulator in the drain end of the channel is reduced from V_G to $V_G - V_D$. This causes the potential difference in Fig. 2.8(c) to reduce until E_i crosses the Fermi level at $V_D \approx V_G - V_T$, and there is no inversion in the drain end of the channel. The channel is said to be *pinched off*. After this point the drain current stays at the saturation value, although in real devices there are effects which cause the drain current to increase slightly also after pinch-off. The drain current, I_D, as a function of V_D and V_G is given by equation 2.1

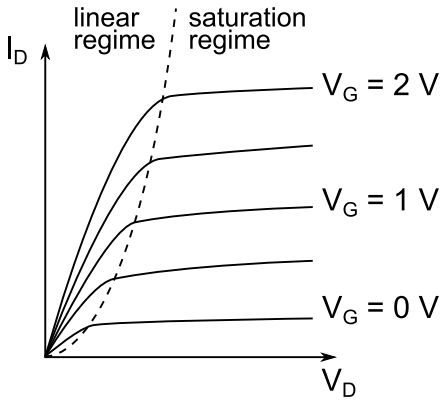

Figure 2.9. *An example of output curves for different gate voltages. Adapted from [33, p. 266]*

in the case where the channel length L is much larger than the insulator thickness d. [33, p. 296; 40]

$$I_D = \frac{\mu W C_i}{L} \left\{ \left(V_G - V_{FB} - 2\frac{\phi_F}{q} - \frac{V_D}{2} \right) V_D - \frac{2}{3} \frac{\sqrt{2\epsilon_s q N_a}}{C_i} \left[\left(V_D + 2\frac{\phi_F}{q} \right)^{3/2} - \left(2\frac{\phi_F}{q} \right)^{3/2} \right] \right\} \tag{2.1}$$

In this equation, W and L are the width and length of the channel, respectively; C_i is the specific capacitance of the insulator; V_{FB} is the voltage required to achieve 'flat-band' conditions; ϕ_F is the difference between the Fermi and intrinsic levels of the semiconductor; ϵ_s is the semiconductor permittivity; q is the electron charge and N_a the semiconductor hole doping concentration. The quantity μ is the *charge carrier mobility*, which describes the speed with which the carriers can move in the semiconductor in an applied electric field. It is a constant for a given material, charge carrier type (electron or hole) and doping concentration. Mobilities in common inorganic semiconductor materials range from 10^2 to 10^5 $\mathrm{cm}^2/(\mathrm{Vs})$. [33]

In the linear region of the output curve, where $V_D \ll (V_G - V_T)$, Eq. 2.1 simplifies to [33]:

$$I_{D,lin} = \frac{W}{L} \mu C_i \left(V_G - V_T \right) V_D \,, \tag{2.2}$$

where the threshold voltage V_T is given by [40]:

$$V_T = 2\frac{\phi_F}{q} + \frac{\sqrt{4\epsilon_s q N_a \phi_F / q}}{C_i} \,. \tag{2.3}$$

This is the expression for threshold voltage in terms of the device parameters.

In the saturation region the drain current I_D ideally no longer depends on the drain voltage. The saturation current can be calculated from

$$I_{D,sat} = \frac{W}{2L} \mu C_i (V_G - V_T)^2 \,. \tag{2.4}$$

This equation is obtained from Eq. 2.1 at $V_D = V_G - V_T$ with simplifications. [33, p. 297].

2.2.3 Transfer characteristics of MISFETs

In addition to output characteristics another important way to examine transistor function is to measure the drain current while sweeping the gate voltage and keeping the drain voltage constant. The result is called a transfer curve. According to Eq. 2.2, the drain current should increase linearly with the gate voltage in the linear region, i.e. when the drain current is low. In the saturation region, the drain current

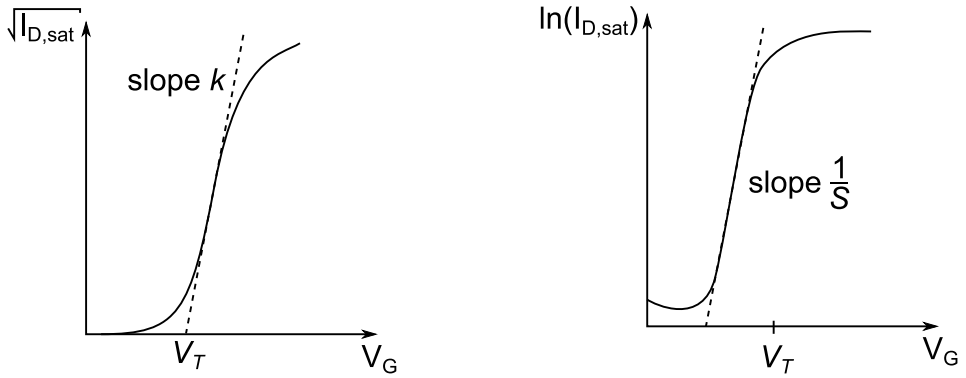

(a) The square root of the transfer curve in the saturation region, i.e. large V_D. Adapted from [33].

(b) The subthreshold slope of a transfer curve. Adapted from [33].

Figure 2.10. *Two ways of plotting the transfer characteristics of MISFETs*

depends on the gate voltage quadratically as in Eq. 2.4. Therefore it is useful to plot the square root of the saturation drain current as a function of the gate voltage:

$$\sqrt{I_{D,sat}} = \sqrt{\frac{W\mu C_i}{2L}}\,(V_G - V_T)\,. \tag{2.5}$$

A representative plot of Eq. 2.5 is given in Fig. 2.10(a). Fitting a straight line to the curve gives the threshold voltage V_T as the V_G axis intercept, and the charge carrier mobility can be calculated from the slope k of the line:

$$\mu = \frac{2Lk^2}{WC_i}\,. \tag{2.6}$$

It is important to note that this equation describes the mobility in the saturation regime.

When the gate voltage is below threshold, the drain current is not zero, but depends exponentially on V_G. If the natural logarithm of the drain current is plotted against V_G, the result is a straight line below V_T. The reciprocal of the slope of this line is called the *subthreshold slope*, S, and it is usually given in units of V/decade. For example, subthreshold slope of 70 mV/decade means that the drain current increases one order of magnitude when the gate voltage is increased by 70 mV. The smaller the value of S, the more sharply the transistor turns on. [33, p. 311]

Another important parameter in FETs is the transconductance, g_m, which describes the change in drain current with respect to change in the gate voltage. It is calculated in the linear (low V_D) and saturation (high V_D) with the following

equations [40]:

$$g_{m,lin} = \frac{\partial I_D}{\partial V_G} = \frac{W}{L}\mu C_i V_D \tag{2.7}$$

$$g_{m,sat} = \frac{\partial I_D}{\partial V_G} = \frac{W}{L}\mu C_i (V_G - V_T) \tag{2.8}$$

A large transconductance implies that a small variation in gate voltage causes a large variation in the drain current, which is a good property for amplification.

2.2.4 The thin-film transistor

The thin-film transistor (TFT) is a type of field-effect transistor where the components are deposited on an insulating substrate, usually glass, as thin films. This is different from the conventional electronic devices, which are fabricated on single-crystal wafers of the semiconductor. The common deposition methods in TFTs cause a large number of defect states in the semiconductor, resulting in a lower mobility for the charge carriers (on the order of 1 $cm^2/(Vs)$ [34]). On the other hand, the semiconductor deposition enables large-area fabrication of circuitry at low cost. TFTs were first invented in 1962 by Weimer, but did not gain popularity until they found use in liquid-crystal displays. [41–43]

The most common semiconductor in thin-film transistors is amorphous silicon, which is prepared by chemical vapor deposition from SiH_4 gas with a pyrolysis reaction. Because the amorphous material does not have a regular lattice, all silicon atoms are not bound to four neighbors as in crystalline silicon. This results in dangling bonds, which are the source for the local or 'trap' states with energies in the band gap. There is also a large concentration of hydrogen atoms left in the amorphous material, which tie up some of the dangling bonds. Amorphous silicon is therefore usually denoted a-Si:H. [42, 44]

An example of TFT structure is depicted in Fig. 2.11. The TFT is different from the MISFET in that it operates in the *accumulation* region, not inversion. The accumulation for p-type semiconductors is depicted in Fig. 2.8(a). For n-type

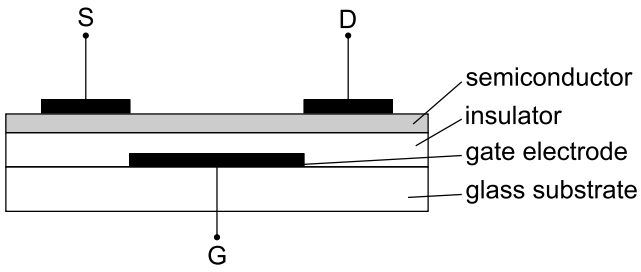

Figure 2.11. *The structure of a thin-film transistor.*

semiconductors, the accumulation of electrons occurs with positive gate voltages. Another difference to the MISFET is that the source and drain electrodes form ohmic contacts directly to the semiconductor. [40]

When an applied gate voltage induces charges in the semiconductor layer, initially most of them fill the many localized states in the band gap. Only at sufficiently high gate voltages electrons begin to fill the conduction band (for p-type semiconductors, holes begin to fill the valence band). This results in an important characteristic of a-Si TFTs: the charge carrier mobility measured by using the field-effect is not constant but a function of the gate voltage. [42]

The equations describing the current-voltage characteristics in the linear region can be simplified slightly from Eq. 2.1 because there is no depletion region:

$$I_D = \frac{W}{L}\mu C_i \left(V_G - V_T - \frac{V_D}{2} \right) V_D \,. \tag{2.9}$$

In this case, the threshold voltage V_T is defined as the gate voltage where the channel conductance ($\frac{\partial I_D}{\partial V_D}$) at low V_D is equal to the conductance of the entire semiconducting layer when there is no gate voltage. In the saturation regime, the drain current is given by the same equation as for MISFETs, that is by Eq. 2.4. [40]

As the magnitude of the drain voltage is increased, the accumulation of charges in the drain end of the channel decreases. The current saturates when the drain voltage is $V_G - V_T$ and a depletion region is formed in the drain end of the channel. Since the mobility is gate voltage dependent – or more accurately charge carrier density dependent – the value for the mobility as calculated from Eq. 2.6 is not necessarily reliable. Instead, Eq. 2.7 should be used. As this equation describes the transconductance in the linear region, $g_{m,lin}$, the mobility at low drain voltages is

$$\mu = \frac{g_{m,lin} L}{W C_i V_D} \,. \tag{2.10}$$

The transconductance can be measured by measuring the drain current as a function of the gate voltage and finding the slope of the linear part of the curve. This method has its drawbacks as well: it is sensitive to limitations in the charge injection at the electrodes. [40, 45]

The structure of TFTs introduces a new figure of merit for the transistor devices: the *on-off* ratio, $|I_{ON}/I_{OFF}|$. It is calculated as the ratio of drain currents in the *on* and *off* states, respectively, at a constant drain voltage. The *on-off* ratio is not relevant in conventional MOSFET devices, since they have a depletion region which separates the source and drain when the transistor is in the off state. In TFTs, the *off* state simply does not have an accumulation of charges in the channel, and the low conductivity of the semiconductor itself ensures that a very low current flows

between the source and drain electrodes. The larger the ratio is, the better the transistor; if there is a substantial leakage current in the off state, the *on-off* ratio is small. The *on-off* ratios of a-Si TFTs are on the order of 10^6–10^8 [34].

2.3 The organic thin-film transistor

The organic field-effect transistor (OFET) was first invented in 1986 by Tsumura et. al. [7]. Their device used poly(hexylthiophene) as the semiconducting layer, and the gate dielectric was inorganic SiO_2. The term OFET is generally used when the active material, i.e. the semiconductor, is organic, despite what the other materials are. The device architecture of the OFET is most commonly that of the thin-film transistor, which is why the terms organic field-effect transistor and organic thin-film transistor (OTFT) are often used synonymously.

Possible applications for OTFTs are as switches in active matrix liquid crystal displays as well as active matrix organic light-emitting diode displays (AMOLEDs) [16] and in simple logic circuits such as smart cards [16] and radio-frequency identification (RFID) tags [45]. They cannot compete in speed with traditional silicon electronics in e.g. microprocessors, but the large area fabrication and inexpensive processing they offer gives them the advantage in the above mentioned and other applications.

2.3.1 Structure and performance of OTFTs

The equations characterizing inorganic, a-Si:H thin film transistors can be adopted to OTFTs since these, too, are based on low-mobility semiconductors and operate in the accumulation regime of FETs. There are also differences: for example, the trap states in amorphous silicon caused by uncompensated bonds do not appear in organic semiconductors due to their molecular nature. There are of course other trap states caused by impurities and the disorder especially in polymeric semiconductors.

The field-effect mobilities in OTFTs are on the order of 1–5 $cm^2/(Vs)$ for small molecules and 0.1–0.6 $cm^2/(Vs)$ for solution-processed microcrystalline polymers [34, 45]. This compares favorably with a-Si TFTs which have mobilities of similar magnitude. OTFTs have the advantage of room-temperature processing. Most OFETs are based on hole transporting, p-type organic semiconductors, but there has been much research into n-type and ambipolar semiconductors that could be used to build e.g. complementary MOS (CMOS) type circuits [34].

Different configurations of OTFT structures are shown in Fig. 2.12. The choice of structure is done according to what is convenient for the materials and deposition methods used. The gate electrode can be either on top or on the bottom of the device; this determines the mutual order of the semiconductor and dielectric layers.

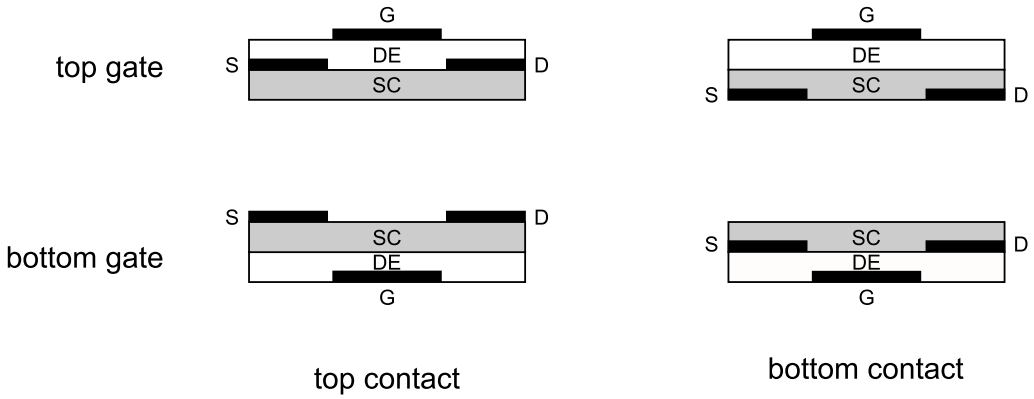

Figure 2.12. *Different configurations for the layers in organic thin-film transistors. "DE" denotes the dielectric and "SC" the semiconductor. Adapted from [46] and [45].*

The source and drain electrodes can be deposited before or after the semiconductor layer; this results in bottom and top contact configurations, respectively.

If the substrate is a doped silicon wafer, it can serve as the bottom gate electrode [46]. Top-gate structures have the advantage of the dielectric layer acting also as a passivation layer for the semiconductor, since many organic semiconductors degrade when exposed to ambient air. When the electrodes are metal, top-contact geometry has been found to offer a lower contact resistance between the semiconductor and the source and drain electrodes. This is because during the deposition the metal penetrates into and mixes with the semiconductor. [45]

A device geometry with a top-contact and bottom-gate or bottom-contact and top-gate configuration is called a staggered geometry. In this structure, the semiconductor-electrode contacts are on the opposite side of the semiconductor layer than the conducting channel. This introduces an additional resistance called *access resistance* between the electrode and the channel, since the semiconductor is very poorly conducting where there is no field-induced charge. [45]

Interface smoothness is important to the function of the OTFT, especially in the interface between the semiconductor and dielectric layers. When fabricating solution-processed semiconductor and dielectric layers, the dissolution of the bottom layer when depositing the top layer may result in interface mixing and increased roughness. This impairs the charge transport of the semiconductor, which happens at the interface to the dielectric. Therefore it is critical to plan the device fabrication in such a way that the solvent of the top layer does not dissolve the bottom layer. [34]

2.3.2 Insulator materials

Initially OFETs were fabricated with the bottom gate structure using a single-crystal silicon wafer as both the substrate and the gate electrode. In this case the dielectric was thermally grown SiO_2. This fabrication method was convenient due to the well-established methods of silicon microelectronic technology. More recently focus has shifted towards organic dielectric materials which, like organic semiconductors, offer the advantage of low-cost, large-area processing. [45]

The capacitance of the dielectric is the most important property of the dielectric layer. The larger the capacitance, the more charges are induced in the semiconductor channel at a given gate voltage. The capacitance is

$$C = \frac{k\epsilon_0 A}{d}\,, \tag{2.11}$$

where k is the insulator dielectric constant (also denoted ϵ_r), ϵ_0 the vacuum dielectric constant, A the electrode surface area and d the thickness of the dielectric. The specific capacitance, C_i, in the equations describing transistor current-voltage characteristics is C/A. High capacitance is beneficial, because it allows larger currents with lower operating voltages [47]. The route to higher capacitance dielectrics can be achieved in two ways: increasing the dielectric constant or decreasing the thickness [45]. As device dimensions such as the channel length L are reduced, the dielectric layer needs to be made thinner as well; the ratio d/L should be less than 0.1 for acceptable *on-off* characteristics [48].

It is well established that charge transport in the semiconductor occurs only in the first few molecular layers of the semiconductor at the dielectric interface. Therefore the properties of the dielectric at the interface are important. If the interface is rough, there are valleys in the semiconductor that can act as charge traps. In bottom-gate devices, a rough interface can also prevent the formation of large crystal domains in the semiconductor. This is of course not relevant in amorphous semiconductors. The interface roughness between two polymers is determined by a balance between the entropy which favors a large surface area and the unfavorable energy of interaction between the materials. [34]

Especially with inorganic dielectrics such as SiO_2 the surface to the semiconductor is often modified with a self-assembled monolayer (SAM). SAMs are formed spontaneously through chemisorption, where one end of the active molecule has a strong interaction with the surface of the substrate. As a result, the surface is covered with molecules that have the same orientation. For example, alkyltrichlorosilanes self-assemble readily on hydroxylated surfaces such as glass and SiO_2. In the interface between the dielectric and the semiconductor, the SAM can induce a dipole moment depending on the terminal group of the molecule. For an electron-rich

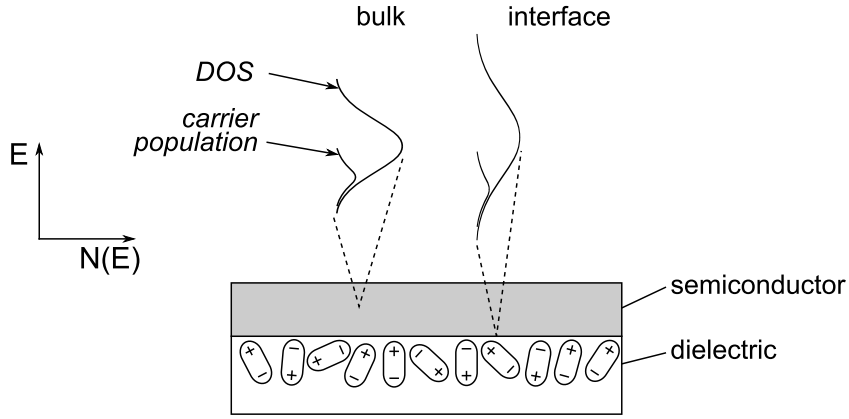

Figure 2.13. *In the Gaussian hopping model, the density of states, N(E), is broadened due to the polar disorder in the dielectric at the interface. Reproduced from [47].*

terminal group that is directed towards the semiconductor, the threshold voltage is shifted to more positive voltages in p-type transport. Similarly, for an electron-withdrawing terminal group, the threshold voltage shifts to a more negative value. [47, 49]

Self-assembled monolayers or multilayers can also be used as dielectric layers themselves, which is a route to achieving very thin dielectric layers [34]. Solution-processed polymer dielectric layers can be made as thin as 50 nm by spin-coating [48]. A challenge especially in very thin layers is that there should be no leakage current from the gate electrode through the dielectric. This means that the dielectric should withstand high voltages over it without breaking down, and that there should not be pinholes or other defects which allow current to pass though it. [34, 47]

The other route to a high capacitance, high dielectric constant (high-k) insulators, have been investigated, but they too have some drawbacks. High-k dielectrics usually contain polar groups that are susceptible to ionic impurities. These can drift in the electric field induced by the gate, creating a hysteresis in the transistor curves. Even without impurities, the randomly oriented dipoles of the dielectric at the semiconductor interface cause energetic disorder, which hinders charge transport. Within the hopping model of transport, where the density of states is usually simplified to a Gaussian distribution, the added disorder broadens the density of states[2]. This is illustrated in Fig. 2.13. The energetic disorder is especially detrimental to amorphous semiconductors that already have a high degree of disorder in their structure. [34, 47]

Polar and ionic groups in the dielectric interface may also act as traps to charge carriers. Such trapping has been found to be one cause for the scarcity of electron-

[2]The density of states (DOS) describes distribution of available states that electrons can occupy against electron energy.

transporting OTFT materials: groups with a higher electron affinity than the semiconductor readily trap electrons. Many studies of semiconducting materials have been and still are conducted with SiO_2 as the gate dielectric. The SiO_2 surface contains many Si−OH groups, which are electron-trapping. Many semiconductors do show n-type transport in other applications than OTFTs, such as light-emitting diodes. One way to reduce the trapping is to use a thin buffer layer such as a SAM between the dielectric and semiconductor. [34]

Examples of frequently used high-k polymer dielectrics include poly(4-vinylphenol) (PVP) and poly(methyl methacrylate) (PMMA), which have dielectric constants 4.5 and 3.5, respectively. Inorganic dielectrics generally have high dielectric constants: for example in SiO_2 $k = 3.9$, in Al_2O_3 $k = 8.4$ and in TiO_2 k is as high as 41. Examples of low-k dielectrics are poly(perfluoroethylene-*co*-butenyl vinyl ether) with $k = 2.1$ and poly(propylene-*co*-(1-butene)) with $k = 2.3$. The choice of dielectric is often a trade-off between the high capacitance that polar, high-k dielectrics offer and the trap-free conduction in devices with a low-k dielectric. [47, 50]

2.3.3 Semiconductor and electrode materials

There are two basic types of organic semiconductors for thin-film transistors: small molecules and polymers. Of these, small molecules perform better, because they can form large crystalline domains, which offer high mobilities. The transport occurs through the conjugated π orbitals, which overlap well in the crystalline material. The most important small molecule semiconductors are pentacene, rubrene and oligomeric thiophene. Small molecules are usually vacuum-deposited, but they can also be deposited from solution. [22, 34]

Polymeric semiconductors have poorer properties in charge transport, but their processability is generally better. Microcrystalline and amorphous polymers both have their advantages. The most common polymer studied in TFT applications is the microcrystalline regioregular poly(3-hexylthiophene) (P3HT), which has very good π–π interaction between adjacent chains in the ordered crystal. Field-effect mobilities of 0.1–0.3 $\mathrm{cm}^2/(\mathrm{Vs})$ have been attained for conventional (non-ion gel) P3HT-OTFTs. [34]

The regioregularity (polymerization by head-to-tail) is extremely important to the conduction properties of P3HT. The deposition conditions also have a significant effect on the mobility in the OTFT, because they control the formation of the crystalline domains. P3HT reacts with oxygen in ambient air, which causes the threshold voltage of the P3HT-OTFT to shift to more positive voltages. This is a result of doping by the oxygen so that there are charges in the channel even at zero gate voltage. [34]

Amorphous polymers such as poly(triarylamine) (PTAA) have also been investi-

gated in OTFT devices. Their advantage is better stability towards ambient conditions compared to e.g. P3HT, but they have lower mobilities, from 10^{-5} to less than 0.01 $cm^2/(Vs)$. Almost all polymer semiconductors are p-type, since efficient n-type transport in OFETs has only been demonstrated for very few polymers. [22]

In choosing electrode materials for OTFTs, the alignment of the energy levels as discussed in Sec. 2.1.3 is essential for good transistor performance. It is also important that the electrode material does not form an oxide layer in ambient conditions, as such a layer introduces an additional barrier for charge injection. Contact resistance between the electrode and the semiconductor is an important quantity in OTFTs, especially when it becomes comparable to the channel resistance. [45, 51]

The most common electrode materials are gold and indium tin oxide (ITO). An organic electrode material, a blend of poly(3,4-ethylenedioxythiophene) and poly(styrenesulfonate) (PEDOT:PSS) is another promising candidate for use as an electrode material, because it is highly conducting compared to other conjugated polymers. However, at high voltages PEDOT:PSS can separate into its components and diffuse into the semiconductor, which can limit its use in devices. [51]

2.4 Ion gels

Ion gels were first demonstrated as gate insulators in organic field-effect transistors in 2007 by the Frisbie group [20]. Solid polymer electrolytes were studied before as gate dielectrics in OFETs, but the switching speeds of these transistors are restricted to only a few hertz [52]. This is due to the low mobility of the salt ions within the solid polymer matrix. Ion gels consist of a polymer matrix swollen with an ionic liquid. The polymer concentration of the gel can be as low as 5 % by weight, allowing the ions to move relatively freely inside the gel.

Ionic liquids are organic salts that are liquid at room temperature. They have many exceptional properties, e.g. high ionic conductivity, chemical inertness and good temperature stability. When an external voltage is applied to the ion gel, electric double layers form rapidly at the electrodes due to the high ionic mobility and relatively low polymer content. They form very thin electric double layers giving rise to a high specific capacitance, which enables transistor function at low voltages. The specific capacitances of ion gels usually range from 1 to 40 $\mu F/cm^2$ [19, 20, 53, 54]. This compares favorably with the specific capacitances of more conventional dielectrics: devices fabricated with SiO_2 and polyimide display specific capacitances of 10 nF/cm^2 [55] and 20 nF/cm^2 [56], respectively. Capacitances this low require high operating voltages, which is not feasible in many applications.

2.4.1 Ionic liquids

Ionic liquids are salts which have unusually low melting points and many of them are liquid at room temperature. They are organic compounds, where at least one of the constituent ions is so large, nonsymmetrical and conformationally flexible that the packing in the solid state is not efficient. This causes the lattice enthalpy to be low, resulting in a low melting point. [57]

Interest in ionic liquids has mainly been as "green solvents" for organic synthesis: their vapor pressures are negligible and they are nonflammable. These liquids have good chemical and thermal stability, and being molten salts, good ionic conductivity [58]. Ionic liquids have also been called "designer solvents" because their properties can be adjusted by choosing different ions [59]. For example, ionic liquids have been studied as solvents for cellulose, an important but poorly soluble biopolymer [60]. Other possible applications include dye-sensitized solar cells [61] and batteries [62].

Charge delocalization in large ions is important to the properties of the ionic liquid [63]. Common cations in ionic liquids are derivatives of nitrogen heterocycles such as imidazolium, pyridinium and pyrrolidinium, as well as quaternary ammonium ions and tetra-alkyl phosphonium ions. By far the most widely used cations are 1,3-dialkyl imidazolium ions. Anions in ionic liquids can be small, such as halogens, or very large, such as the popular bis(trifluoromethylsulfonyl)imide anion. Other anions include trifluoromethane sulfonate, hexafluorophosphate and tetrafluoroborate. [64, p. 3.] The first room-temperature ionic liquid discovered was ethyl ammonium nitrate (melting point 12 °C), which was synthesized in 1914 by Walden [65].

The ionic liquid used in this work is 1-methyl-3-ethylimidazolium bis(trifluoromethylsulfonyl)imide or EMITFSI whose components are illustrated in Fig. 2.14. In general, 1,3-dialkylimidazolium$^+$-TFSI$^-$ salts have a good stability with regard to water, air and temperature as well as a wide electrochemical window [3]. Their viscosities are low compared to simpler halogen imidazolium salts, which leads to

[3]The electrochemical window means the difference in anodic and cathodic decomposition potentials, in volts [66]

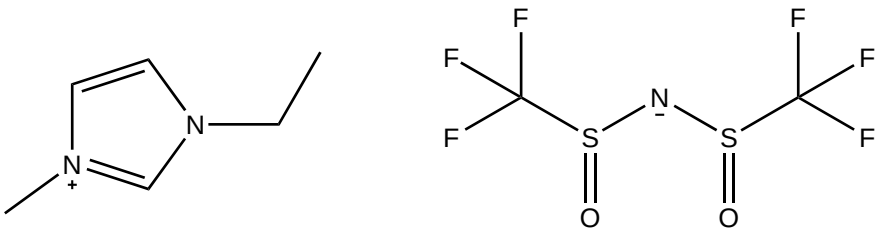

Figure 2.14. *The components of 1-methyl-3-ethylimidazolium bis(trifluoromethylsulfonyl)imide, EMITFSI.*

higher ionic conductivity. [64, p. 56.] The stability is the result of delocalized and shielded charge. In the imidazolium cation, the positive charge is delocalized on the nitrogen atoms equally [67, p. 1165]. The negative charge of the $TFSI^-$ anion nitrogen is delocalized on the neighboring sulfur atoms, but not significantly on the oxygen atoms. These along with the terminal triluoromethyl groups provide shielding from surrounding cations. [64, p. 4.]

2.4.2 Formation of ion gels

A gel is generally defined as a polymer network swollen with a liquid [68]. The liquid fills the space between the elastic polymer chains; the liquid can be thought of as being dissolved in the polymer. The consistency of gels is something between a solid and a liquid. They have the cohesive properties of solids, but are soft and can deform significantly under stress. They also have the diffusive transport properties of liquids, which makes them interesting for certain applications, such as electrochemical energy storage devices. [59, 69, 70]

Gelation can be brought on chemically by polymerization with chemical cross-links or physically by non-covalent bonding, e.g. phase separation or microcrystallization. For chemical cross-linking gelation is thermoset, but for physical cross-linking it is thermoreversible. In physically cross-linked gels, the number of cross-linking points depends on temperature, pressure and time. [68]

Ionic liquid based gels have been proposed as new alternatives for polymer electrolyte materials. Previously ion-conducting polymer electrolytes have been prepared by dissolving high melting point salts in polymers. The difficulty in these materials has been the limited ionic mobility: the ionic motion is coupled with the segmental motion of the polymers, but the glass transition temperature of the mixture increases with increasing salt concentration. Using ionic liquids to make polymer electrolytes enables both high ion concentration and high ion mobility; this is because the ions are in the liquid form themselves. The resulting ion gel can even be prepared by in situ polymerization of the gel polymer network, since the solvent properties of the ionic liquids are often good. [71]

Gels prepared from ionic liquids and block copolymers are based on non-covalent bonding of the polymer blocks. Compared with chemical cross-linking, this enables gelation at relatively low polymer weight fractions [73]. The ion gel used in this work contains an ABA triblock copolymer where the A blocks are polystyrene (PS) and B blocks poly(methyl methacrylate) (PMMA). The PS blocks are not miscible with the ionic liquid EMITFSI, but the PMMA blocks are. This causes a phase separation when the ionic liquid and polymer are mixed [72].

Usually gel preparation is carried out by dissolving both ionic liquid and polymer in a cosolvent, which is then evaporated, leaving the self-assembled gel. The gel

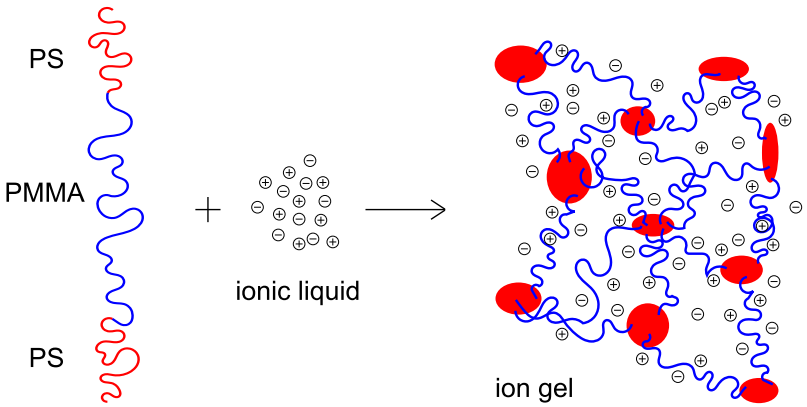

Figure 2.15. *The formation of an ion gel from PS-b-PMMA-b-PS block copolymer and ionic liquid. The red PS blocks separate from the liquid to form solid particles. Adapted from [72].*

formation is depicted in Fig. 2.15. The mesh size of the polymer network ranges from 10 to 100 nm, which is much larger than the ions. This enables the ions to move inside the gel. The properties of the gel can be tuned by choosing different ionic liquids and polymers or by changing the polymer block lengths. With suitable choices, the polymer end blocks can be made soluble at elevated temperatures. This enables thermoreversible gelation. [72]

2.4.3 Electrical properties of ionic liquids and ion gels

The behavior of ionic liquids and ion gels in an external electric field is important to their use in electronic devices. The ionic conductivity represents the ease with which the ions move in the electrolyte. In field-effect transistor dielectrics, an important parameter is the capacitance of the ionic liquid or gel. The electrochemical stability is also of great importance in this application, since electrochemical reactions cause leakage currents through the dielectric.

Ionic conductivity

The mobility of ions through the polymer network gives rise to ionic conductivity in the gel. Specific conductivities of pure ionic liquids usually range from 0.1 to 18 mS/cm. The introduction of a polymer of course reduces the conductivity. For example, a PMMA content of 30 % by weight decreases the conductivity of EMITFSI to 5.7 mS/cm from the pure ionic liquid conductivity of 9.4 mS/cm. [71, 74, 75]

One important factor in ionic liquid conductivity is water as an impurity: it increases the conductivity dramatically. One reason for this is that water decreases the viscosity, allowing the ions to move more freely [76, 77]. Ionic liquid miscibility

with water depends mostly on the anion; $TFSI^-$ salts for example are not water-soluble. However, even hydrophobic ionic liquids can be remarkably hygroscopic [78]. The saturation water content of EMITFSI at 20 °C is 1.4 % by weight [75].

Another factor affecting the conductivity is that bulk ionic liquids are not completely dissociated into ions, but form aggregates and nanometer-size structures where the ions are bonded through hydrogen bonds and dispersive forces as well as the electrostatic attraction of the ions [71, 79]. Because of the aggregation, in EMITFSI for example only 30 to 50 % of the ions contribute to the ionic current [71].

In their study of in-situ-polymerized PMMA-EMITFSI ion gel, Susan et. al. [71] found that there is an interaction between the $TFSI^-$ anion and the polymer, which lessens the aggregation of the ionic liquid. This in turn improves the cation mobility, leading to a higher conductivity. It can be expected that a similar interaction occurs in EMITFSI-block copolymer gels where the middle block is PMMA.

Capacitance and leakage in ion gels

When an ion gel is placed between two metal electrodes and a voltage is applied between them, the ions migrate to the electrodes of opposite sign (Fig. 2.16). Provided that the applied voltage is not so large that redox reactions take place, the ions form *electric double layers* with the equal, but opposite charges in the metal electrodes [80].

This kind of a structure is called an electrochemical capacitor. It can be used for energy storage, since the charged layers persist when the circuit is opened [80]. Unlike a traditional capacitor, the capacitance is not dependent on the thickness of the electrolyte layer, but the thickness of the electric double layer, which is in

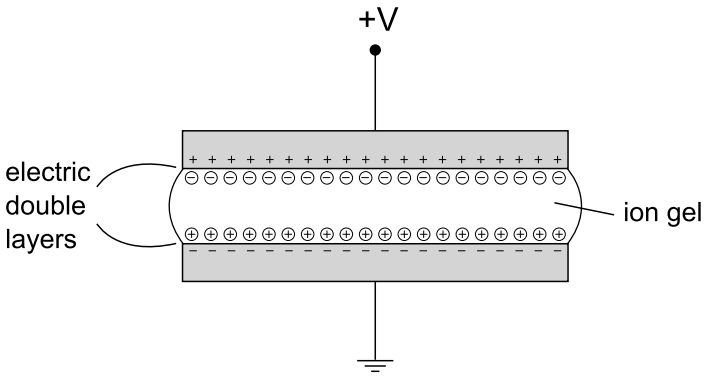

Figure 2.16. *The formation of electric double layers at electrode interfaces in a capacitor with an ion gel as dielectric.*

Ångström scale [81]. The specific capacitance C_i of the capacitor is

$$C_i = \frac{C}{A} = \frac{\varepsilon_r \varepsilon_0}{d}\,. \tag{2.12}$$

Because of the extremely small electric double layer charge separation d, the capacitance can be quite large: the specific capacitances of electric double layers are usually 5–40 µF/cm^2 depending on the electrolyte [53, 81]. The specific capacitance of a common inorganic dielectric SiO_2 with a thickness of 150 nm is only 20 nF/cm^2 [20].

The capacitance is frequency-dependent. The mobility of the ions through the gel limits the speed at which the electric double layers can be formed, and therefore at high frequencies the capacitance can be significantly less than at low frequencies. For example, a gel composed of EMITFSI and PS-*b*-PMMA-*b*-PS has a specific capacitance of 30 µF/cm^2 at 10 Hz, but already at 10 kHz it is reduced to less than 10 µF/cm^2 [19]. This is, however, still much better than many conventional dielectric materials, where the capacitances are on the order of 10 nF/cm^2 [55].

The electrochemical window of the electrolyte is an important parameter in a capacitance-type stucture. It means the width of the potential interval in which there is no appreciable Faradaic current, i.e. electrolysis (anodic or cathodic reactions) does not happen in significant quantities. Static leak currents through an electrochemical capacitor are mostly Faradaic currents [82]. Impurities like water can have a smaller electrochemical window and therefore contribute to leakage [63]; for water the electrochemical window is only 1.2 V [83]. Ionic liquids generally have wide electrochemical windows, especially the $TFSI^-$ anion which is oxidized only at relatively high anodic potentials. The electrochemical window for EMITFSI is over 4 V. [74]

2.4.4 Ion gels as dielectrics in OFETs

The high capacitance of ion gels enables high induced charge densities in ion gel gated organic field-effect transistors at low voltages. When the semiconductor is p-type, applying a negative gate voltage creates electric double layers at the gel-electrode and gel-semiconductor interfaces as depicted in Fig. 2.17. The negative ions in the gel accumulating on the semiconductor interface induce positive charges, holes, in the semiconductor channel. The channel becomes conductive and current flows between the source and drain electrodes.

The doping mechanism in electrolyte-gated OFETs is not necessarily purely field-effect: the anions may be able to penetrate into the semiconductor layer resulting in electrochemical doping. This has been studied with ATR-IR experiments and the mathematical modeling of ion diffusion, where the findings were that at high fre-

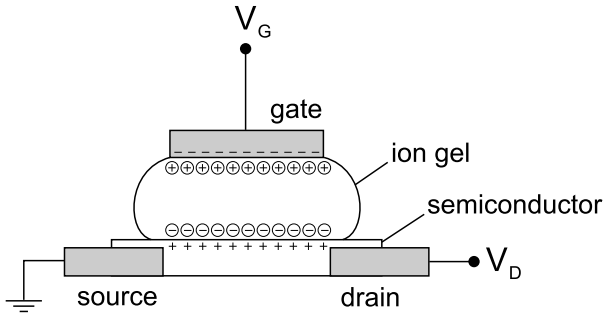

Figure 2.17. *A top-gate OFET with an ion gel dielectric layer.*

quencies (> 1 kHz) the mechanism is primarily electrostatic i.e. field-effect, whereas electrochemical doping comes into play at low frequencies. The limiting factor is the ion diffusion speed into the semiconductor. The equations describing the current-voltage characteristics of thin-film transistors (Sec. 2.2) are valid also for electrochemical transistor operation. [19]

The first ion gel gated transistors were fabricated using a gel formed from the ionic liquid $BMIPF_6$ and the block copolymer polystyrene-*b*-poly(ethylene oxide)-*b*-polystyrene (PS-*b*-PEO-*b*-PS) [20]. In later studies, gels have also been prepared from the ionic liquids EMITFSI and $EMIOctOSO_3$ and the block copolymer PS-*b*-PMMA-*b*-PS (Fig. 2.18) [19, 53, 54]. The latest research has been focused on the combination of EMITFSI and PS-*b*-PMMA-*b*-PS, which has been found to have better properties compared to others [14, 19, 84, 85].

The charge carrier mobilities in the devices utilizing P3HT or similar polymers as semiconductor have been on the order of $1\ \mathrm{cm}^2/(\mathrm{Vs})$, measured with gate voltage sweeping rates of $50...75\ \mathrm{mV/s}$ [19, 53, 54]. This compares favorably with the mobilities in polymer semiconductor OFETs with conventional dielectrics, which are

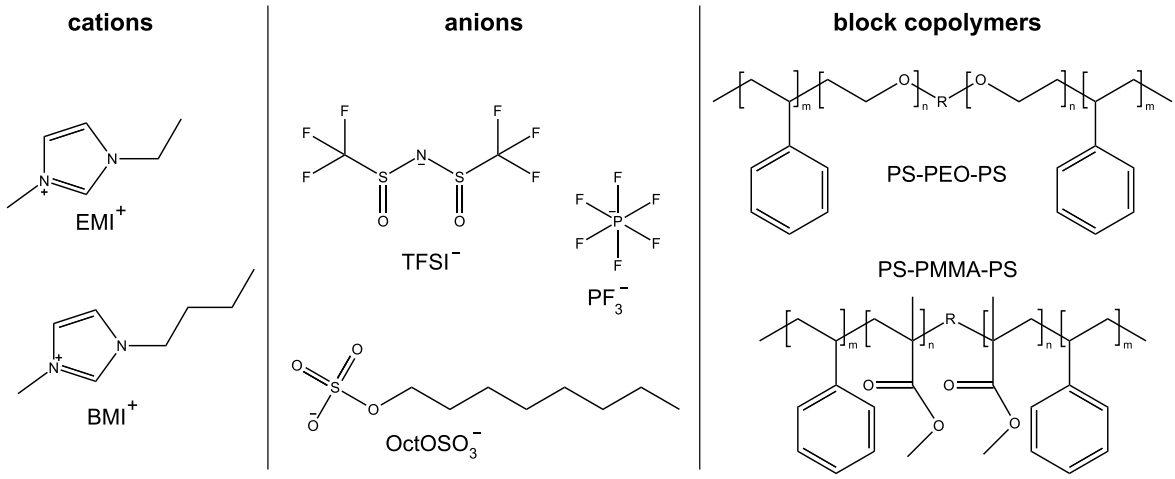

Figure 2.18. *The materials used in ion gel OFETs.*

on the order of 0.1 $cm^2/(Vs)$ [86]. Ion gel gated transistors have also been prepared using ambipolar carbon nanotube or graphene semiconductors. In these devices the mobilities have reached over 20 $cm^2/(Vs)$ for C-nanotubes [84] and over 300 $cm^2/(Vs)$ for graphene [85].

The large capacitance of the ion gel offers many advantages. The large charge density induced in the channel gives rise to higher charge carrier mobilities due to increased trap-filling in the semiconductor [54]. Because the capacitance stems from the electric double layers, the thickness of the gel layer itself doesn't significantly affect the capacitance [14]. This makes layer deposition easier, since the thickness does not need to be controlled closely. The gate electrode doesn't even need to be exactly on top of the channel: the high polarizability of the gel makes it possible to fabricate transistors where the gate is offset from the channel by as much as 60 µm [52, 54]. Again this eases the device fabrication.

A major drawback of ion gel gated transistors is their slow polarization time: the switching speed is limited by the ion movement through the gel [54]. Ion gel dielectrics are however better than previous solid polymer electrolytes, where the maximum switching speed has been estimated to be a few hundred hertz [52]. The maximum switching speed for ion gel transistors is approximately 1 MHz, when the minimum time for electric double layer formation is estimated as 1 µs [14].

The aim of organic and printed electronics to produce low-cost flexible components presents another challenge when studying ion gels as dielectrics: electropositive metals such as copper can easily oxidize when in contact with an electrolyte at positive biases. Therefore only expensive noble metals such as gold, platinum or palladium can be used as metal electrodes. [14] This can be circumvented by using conductive polymers [54] or certain carbon-based conductors [14] as electrode materials. Organic semiconductors on the other hand are usually stable towards electrolytes [14].

Ion gel gated transistors have another potential disadvantage concerning power consumption: in addition to their high *on* currents, they usually also have large *off* currents due to both static and dynamic leakage. One important source of static leakage current is water (as well as other impurities), which can cause electrochemical reactions at the electrodes. Dynamic leakage currents derive from the large capacitance of the ion gel which leads to large displacement currents when the transistor is switched. This can be addressed by decreasing the device size. [14, 54]

3 MATERIALS AND METHODS

3.1 Materials

The ionic liquid used in the ion gel was 1-methyl-3-ethylimidazolium bis(trifluoromethylsulfonyl)-imide (EMITFSI), which was purchased from VWR. The block copolymer polystyrene-*b*-poly(methyl methacrylate)-*b*-polystyrene (SMS) was purchased from Polymer Source. The molecular weight of the PS blocks was 10 000 g/mol and the PMMA blocks 45 000 g/mol. The polydispersity index of the polymer was 1.5. The chemicals were used as received.

The cosolvent used in the gel preparation was ethyl acetate (EtAc). Before use in OFET ion gels, it was dried with Na_2SO_4 overnight and filtered just before use. The EtAc was not dried when formulating the capacitance test structure gels. All glass containers and tools were dried in an oven at 120 °C for approximately 2 hours before use. The ionic liquid and the gel solutions were stored in a desiccator.

The semiconductor chosen for the ion gel gated transistors was poly(triarylamine) (PTAA), because it is very stable in air. The stability offers facile preparation and better stability of the finished device. The PTAA used was a commercial solution in *o*-xylene/tetralin and it was used as received.

The substrate used was a poly(ethylene terephthalate) (PET) film, Melinex ST506 from Dupont Teijin Films. The thickness of the film was 125 µm. The film is flexible and it can withstand temperatures up to 150 °C without deformation. It is also resistant to many solvents.

Poly(methyl methacrylate) PMMA was used as a dielectric in reference samples. It was in a solution of 1:1 toluene and ethyl acetate where the concentration of PMMA was 13 % by weight. The solution was stirred overnight before use to ensure proper dissolution.

3.2 Sample preparation

All sample preparation steps were carried out in a dust-free environment, which is non-certified but close to ISO 14644-1 class 5. Care was taken to store the samples and materials in closed containers or bags with desiccant.

3.2.1 Ion gel formulation

The ion gels were prepared using stock solutions of EMITFSI and PS-*b*-PMMA-*b*-PS (SMS) in EtAc. The amounts of materials and concentrations of the stock solutions are presented in Table 3.1. The stock solutions were stirred overnight in room temperature. The solution containers were inside a larger container which had desiccant at the bottom, to ensure a drier environment for the solution.

Table 3.1. *The preparation of the stock solutions for the ion gels.*

	SMS (mg)	EMITFSI (mg)	EtAc (mg)	wt.% in solution
gel for capacitors	21.4		878.7	2
		114.7	899.3	11
gel for transistor	41.3		1827.6	2
		285.1	1880.9	13

Table 3.2. *The preparation of the ion gel solutions.*

	SMS stock solution (mg)	EMITFSI stock solution (mg)	wt.% of polymer in finished gel
capacitor 1	81.3	86.5	16
capacitor 2	80.9	71.9	20
capacitor 3	86.7	62.3	23
transistor	180.8	160.2	16

The ion gel solutions were prepared by combining the stock solutions as presented in Table 3.2. The combined ion gel solution was stirred for approximately an hour, after which it was poured onto a warm and dry clock glass and the solvent was evaporated. The result was a clear gel, which was further dried in vacuum at 35 °C for an hour.

3.2.2 Electrode and semiconductor layers

Au electrodes were vacuum evaporated through a shadow mask on the substrate. The evaporation of the electrodes was done at the TUT ORC laboratory. The layer growth rate was 0.2 nm/s and the pressure during evaporation 10^{-6} mbar. The resulting Au layer thickness was 50 nm.

The electrodes for the capacitor structures were 390 µm wide and 6 mm long strips of Au with contact pads on each end. In the transistor structures, the channel width was 4000 µm and length 20 µm. One sample contained four source-drain structures. The Au gate electrode was evaporated on a separate PET film and had width 1 mm and length 21 mm with a contact pad at the end. The gate electrode of the reference

transistor structure was evaporated onto the dielectric layer using the same shadow mask.

PTAA was spin-coated on the evaporated source-drain structure. Before spin-coating, the substrate was rinsed with deionized water and blown dry with pressurized air. The rotation rate was 500 rpm for 10 s, then 2000 rpm for 60 s. The sample was first left to evaporate the solvent in ambient air for 5 min at room temperature and then cured in the oven at 115 °C in air for 5 min. The sample was let cool slowly to room temperature in ambient air.

3.2.3 Sample assembly

For the capacitor test structures, the ion gel was pasted by hand onto an electrode and another one was pressed on top of it upside down, perpendicular to the bottom electrode. To get a measurement probe contact to the top electrode, Ag flake paint was deposited under one of the contact pads so that the paint was partly visible from underneath the top electrode. The Ag paint was deposited carefully in such a way that it was not in contact with the gel or the bottom electrode. The top electrode was secured in place using tape strips. The Ag paint was left to dry well before measurement.

Before the transistor structure assembly, the gate electrode and the source-drain structures were first kept in the vacuum heater as the gel was dried there at 35 °C for an hour. The gate electrode substrate had tape strips on each side of the electrode for height control of the gel layer. The ion gel was pasted by hand on the gate electrode and the components were placed in vacuum at 35 °C for another hour. The gate electrode was pressed upside down on top of the channel and Ag paint was used as in the capacitor structures to get a probe contact to the top gate electrode.

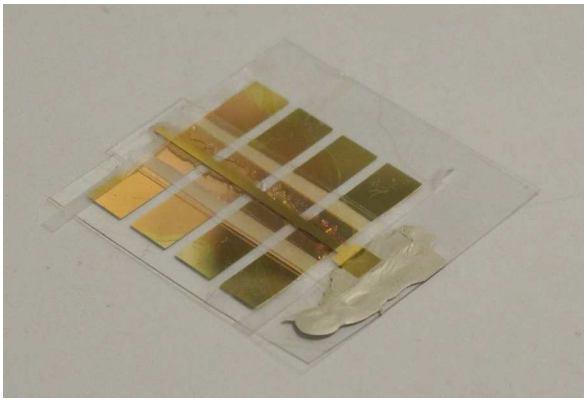

Figure 3.1. *An ion gel transistor sample. The sample contains four transistors: the channels are aligned in such a way that the gate electrode is the same for all of them. The tape strips on the sides of the gate help control the thickness of the gel layer. The Ag paint enables contact to the upside-down gate electrode.*

An example of a sample structure is shown in Fig. 3.1. The finished ion gel samples were stored in an airtight plastic bag with desiccant inside.

A reference sample was prepared with PMMA as a gate dielectric. The PMMA was spin-coated on top of the PTAA layer. The rotation rate was 2000 rpm and its duration 60 s. The solvent was dried at room temperature in air for 5 min, then at 115 °C in air for 5 min. The gate electrode was vacuum evaporated on top of the channel. The shape and size of the resulting transistor sample was identical to that of the ion gel transistor, the only difference being the insulator and gate electrode deposition methods.

3.3 Sample characterization

3.3.1 Capacitance measurements

The capacitances of the samples were determined using a network analyzer (Hewlett Packard 8752A) at frequency range 300 kHz–40 MHz. The lowest frequency available to the network analyzer is 300 kHz, so the results at low frequencies have some error. The lower-frequency capacitance was estimated from the capacitive current using an oscilloscope (Tektronix DPO4104) and a signal generator (Keithley 3390). This setup was tested with known capacitors to determine the range of frequencies where it gave correct results: the range was found to be quite narrow, 10^3–10^4 Hz.

The low-frequency limit or 'DC' capacitance was evaluated from an RC circuit using the oscilloscope and signal generator. The load resistance R was 10.16 kΩ. The input was a square wave with the time interval between signal changes much larger than the time constant τ of the circuit. The voltage over the capacitor was measured.

The leakage current through the capacitors was determined using a semiconductor parameter analyzer (Agilent 4155B). The leakage current was first measured from 0 V to +2 V and back, then from 0 V to –2 V and back. This was done to prevent hysteresis from complicating the results. The measurement speed was low, 20 mV/s.

The capacitance of the reference sample PMMA layer was estimated by measuring the capacitance between the source and gate electrodes and between the source and drain electrodes. The overlap area of the electrodes was measured using a microscope. This measurement was done with the network analyzer at the lowest frequency available (300 kHz) and the average from the source and drain side measurements was calculated.

3.3.2 Transistor IV-analysis

The transistor output and transfer characteristics were measured with the semiconductor parameter analyzer. Because of the moisture sensitivity of the ionic liquid, the ion gel OTFT was measured using a probe system built inside a desiccator (Fig. 3.2). The sample was placed in the desiccator overnight and measured the next day. The reference transistor was measured inside a metal box to decrease outside interference. The currents involved in the ion gel gated transistor measurement were large, so the shielding was not deemed necessary in this case. The source terminal was connected to the ground.

The voltage range in the output measurements for the ion gel gated transistors was from +1 V to –1.5 V between the source and drain. The gate voltages were selected from the same range. The transfer measurements were done with the same voltage range as the output measurements. The measurement speed was very slow due to the ion gel: the sweep speed was 20 mV/s. In the reference OTFT measurements the voltage range used was from +10 V to –30 V. Since hysteresis, such as that in the ion gel transistors, was not expected in the reference sample, the measurement speed was high, i.e. 5 V/s.

The switching properties of the ion gel transistor were examined with a circuit depicted in Fig. 3.3. The input was a square wave from the signal generator with frequencies 10 Hz, 100 Hz and 1 kHz. The –1 V supply voltage at the drain electrode was obtained from a power source (Agilent E3631A). The output voltage over the 10 MΩ load resistor was monitored with the oscilloscope. All measurement devices were connected to a common ground.

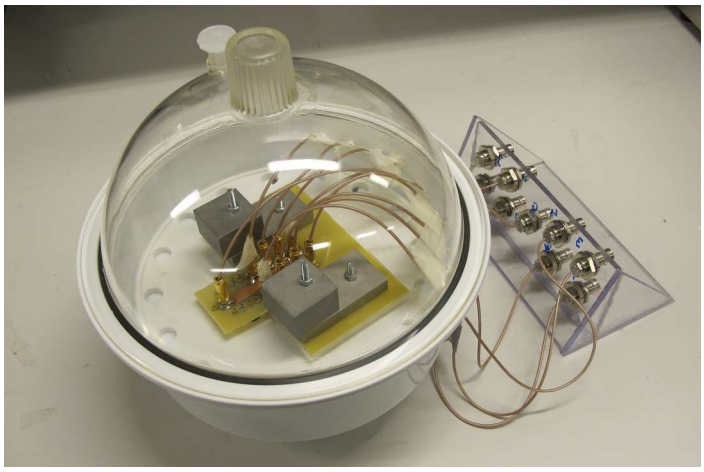

Figure 3.2. *The measurement desiccator with a probe system inside. The probe system was built in such a way that the desiccator did not need to be opened to change the probe position on the sample. Instead all four transistors on the same sample could be measured by changing the input cables.*

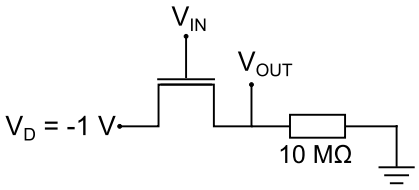

Figure 3.3. *The measurement setup circuit diagram for testing the switching properties of the ion gel gated OTFT.*

When the ion gel transistors were measured, a colour change was observed. To examine it more closely, a transistor was disassembled and the ion gel was rinsed off the semiconductor with ethyl acetate. The color remained on the semiconductor in the area that had been in contact with the ion gel.

4 RESULTS AND DISCUSSION

4.1 Capacitance of the ion gel

The specific capacitance of the gel was determined from the measured capacitance of the test structures by dividing it with the area of the capacitor. The width of the Au strips was 390 µm, which means the area of overlap of the perpendicular strips was $A = 0.001521\,\mathrm{cm}^2$.

There is, however, some uncertainty in the area: the electric double layers in the ion gel may extend further outside the vertical overlap area of the Au strips because of the migration of the ions in the gel. This is illustrated in Fig. 4.1 for a cross-section of the structure along one of the electrodes. In the figure, the length on the top electrode where ions migrate to is larger than the width of the bottom electrode. In the direction perpendicular to the page, the situation is reversed.

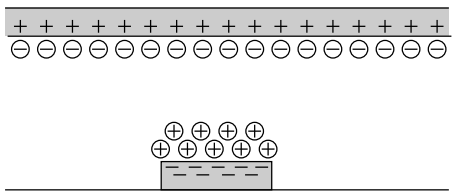

Figure 4.1. *A source of uncertainty in the ion gel capacitance determination. The gray parts are the electrodes and the area between them is the ion gel.*

This may cause the measured capacitance of the ion gel to be larger than it actually is, because the actual area where the charges are accumulated may be larger than the vertical overlap area. The method for the capacitance determination was however taken to be accurate enough for the purposes of this work. In the transistor structure, a similar effect would probably not be relevant, because the gate electrode overlap with the source and drain is in any case very large, causing a charge accumulation in the semiconductor on top of the electrodes. Because of the poor conduction in the semiconductor compared to the metal electrode, current will go through the latter, meaning that the channel area is the only one where the semiconductor charge matters.

4.1.1 Frequency dependence of the capacitance

The capacitance was measured for gels with different polymer concentrations at different frequencies and the results are plotted in Fig. 4.2. At frequencies below 1 MHz, the specific capacitance of the gels is approximately 5 µF/cm^2. Above 1 MHz, there is a sharp decline in the capacitance. This is in line with results in the literature [19, 55].

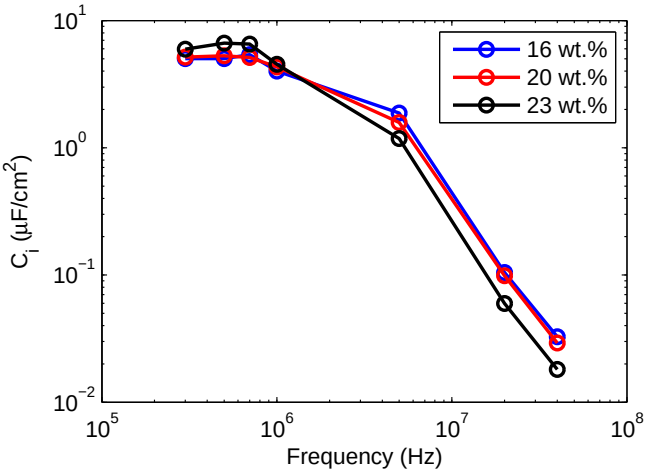

Figure 4.2. *The specific capacitance of the ion gels as a function of frequency.*

There is no significant difference in the specific capacitance of the gels with different polymer concentrations. The gel with the highest concentration has a slightly higher capacitance at lower frequencies, but its capacitance declines more steeply when the frequency increases. This is expected since a higher polymer concentration means the ion movement in the gel is more obstructed.

The results from the capacitive current measurements are plotted in Fig. 4.3 for the gel that had polymer concentration 23 wt.%. The range at which the setup was determined to be accurate enough was 10^3–10^4 Hz. At 10^3 Hz the capacitance was 11 µF/cm^2 and at 10^4 Hz it was 6 µF/cm^2. Within this very specific range, the measured capacitances agree with the results obtained with the network analyzer.

The 'DC' capacitance was evaluated from the time constant $\tau = RC$ of an RC circuit. The time constant is defined as the time it takes for the voltage over the capacitor to fall to $1/e$ of the maximum value. The measured τ was 290 µs, which gives a capacitance of

$$C = \frac{\tau}{R} = \frac{290 \cdot 10^{-6}\,\mathrm{s}}{10\,160\,\Omega} = 0.0285433 \cdot 10^{-6}\,\mathrm{F}$$

and dividing the capacitance with the capacitor area gives 19 µF/cm^2. This result fits the trend of the results in Fig. 4.3 well, since this value of the capacitance can be thought of as the low-frequency limit.

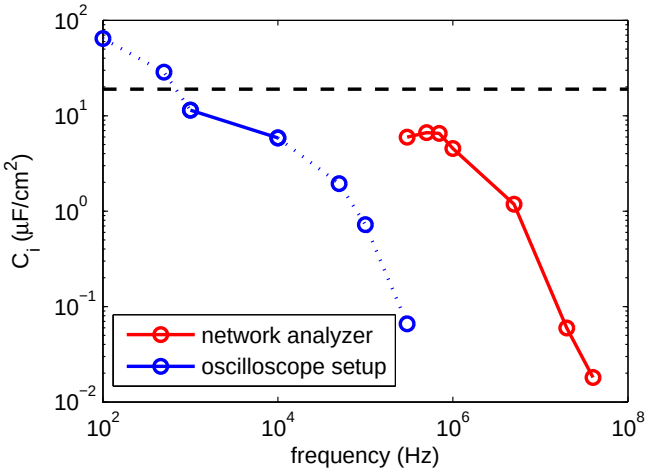

Figure 4.3. *The capacitance of the gel with 23 wt.% polymer as measured with two different setups. The dotted line indicates the points where the measurement setup did not give correct results when testing with known capacitors. The dashed line is the level of the 'DC' capacitance.*

4.1.2 Leakage

The leakage through the ion gel capacitors was measured and the result is plotted in Fig. 4.4 as the current density when the capacitor area is 0.1521 mm^2. The current stays below $2 \cdot 10^{-4}$ A/cm^2 (approximately 0.3 µA) until 1.5 V, but at 2 V the leakage current begins to increase more rapidly. The reason is likely to be water impurity, which has a smaller electrochemical window than the ionic liquid.

The magnitude of the leakage current can be used to estimate the performance as a gate dielectric. The area of the gate electrode overlapping the source and drain

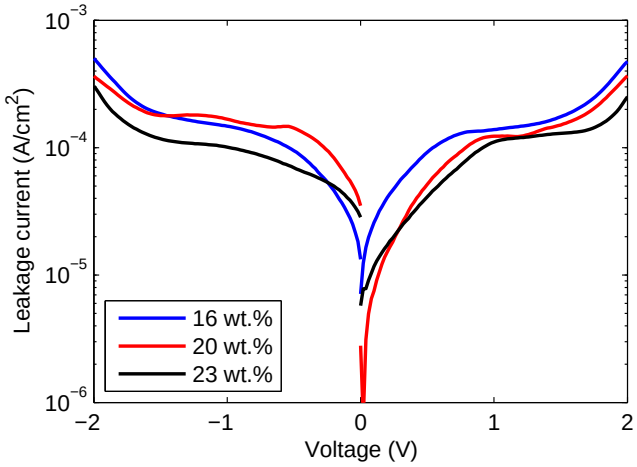

Figure 4.4. *Leakage current density through the capacitor structures. The voltage was sweeped from 0 V to 2 V, then back to 0 V and to –2 V; the return sweep is not plotted. The speed of the measurement was 20 mV/s.*

in the transistor structures is approximately 0.04 cm^2 given the gate width 1 mm and channel width 4 mm. At a current density of $1 \cdot 10^{-4}$ A/cm^2, this implies a leakage current of 4 µA, which is approximately an order of magnitude lower than the output current of the transistors, which is examined in the next section.

There is some correlation between the polymer content in the gel and the leakage current magnitude, although it was not much. This is expected, because as the polymer concentration is increased, the mobility of the ionic liquid as well as the water impurity in the gel is decreased.

4.2 Ion gel gated OTFTs

The finished ion gel transistors had a top gate, bottom contact structure depicted in Fig. 2.12. The lowest polymer concentration was chosen in order to have fast switching properties and because there was no significant difference between the different concentrations in terms of capacitance and leakage. The ion gel gated transistor was measured for the output and transfer characteristics. A very slow measurement speed was used in order to get clear curves: although the capacitance versus frequency measurements indicate that the ion gel capacitor can switch in 1 µs, hysteresis was found to be very sensitive to measurement speed. Extra bumps in the curves moved when the measurement was done faster. The origin of much of the hysteresis appeared to be water impurity.

4.2.1 Output characteristics of the ion gel OTFT

The output of the ion gel gated transistors was measured at different gate voltages and the results are presented in Fig. 4.5 along with the gate leakage currents in the measurement. There is considerable hysteresis between the forward and backward sweeps, and the output curve at –1.5 V has an additional "bump" in the current at saturation voltage. The very different shapes of the forward and backward curves suggest that the reason for this is electrochemical reactions of water impurity.

The leakage current through the gate electrode is at its largest one order of magnitude below the drain current. According to IEEE standards [87] the leakage of an acceptable OFET should be at minimum two orders of magnitude below the drain current. Most of the output curves do meet this requirement, but just barely.

The largest leakage can be seen when the gate voltage is +1 V. The reason may be that the voltage across the ion gel is more than 2 V as the drain voltage is decreased towards –1.5 V. At negative gate voltages the leakage currents are much lower. There is however some effect with the output at gate voltage –1.5 V that causes the leakage to increase. The reason may be related to hysteresis in the measurement, since the drain voltage sweep was begun from +1 V.

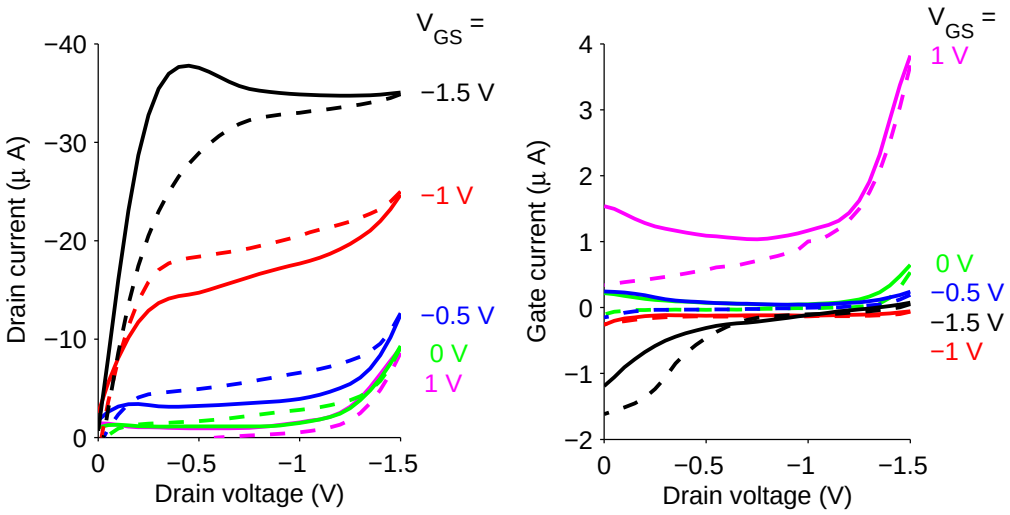

Figure 4.5. *The output characteristics and gate leakage of the ion gel gated OTFTs. The solid line indicates forward sweep from 0 V to –1.5 V and the dashed line the backward sweep. The plot on the left is the leakage current through the gate electrode. The speed of the measurement was 20 mV/s.*

An interesting effect can be seen when the drain voltage is large, –1.5 V: the drain current begins to increase even for the cases where the gate voltage is zero or positive. Comparing with the gate leakage current plot, it can be seen that this extra current flows between the drain and source electrodes, and it is not leakage through the gate. A possible reason for this is leakage between the source and the drain through the ion gel. The channel length is much smaller than the thickness of the ion gel, and there is leakage through the gel from the gate electrode; therefore it is reasonable to assume that the lateral leakage is also possible.

4.2.2 Transfer characteristics of the ion gel OTFT

The transfer characteristics of the ion gel gated transistors were measured for different drain voltages and the results are presented in Fig. 4.6 for drain voltages –0.5 V and –1 V. Since the transfer curves are in the saturation region, the square root of the drain current forward sweep is also plotted.

In the linear region (low V_D) the transistor switching on was masked by hysteresis so strongly that determining the mobility using Eq. 2.10 was not possible. The transfer curve with drain voltage –1.5 V displayed too much leakage to use in mobility calculations. The leakage in this case was mostly between the source and drain electrodes, even with zero or positive gate voltage. The same effect was seen in the output curves in Fig. 4.5 at drain voltage –1.5 V.

To obtain an estimate of the mobility, a straight line was fitted to the square

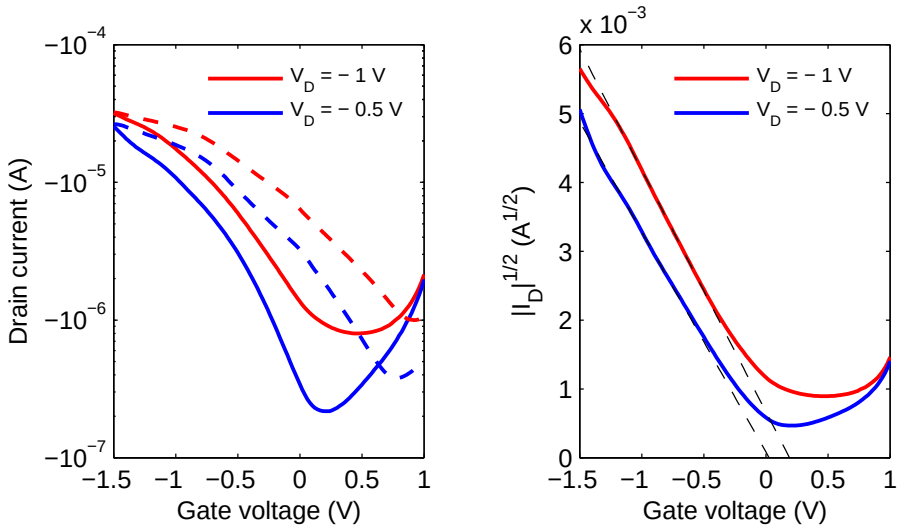

Figure 4.6. *Transfer characteristics of the ion gel gated OTFTs. The plot on the left shows the drain current as a function of the gate voltage at two different drain voltages. The solid lines were measured in the forward direction (from +1 V to –1.5 V) and the dashed lines in the reverse direction. The plot on the right shows the square root of the drain current and the fitted lines. The measurement speed was 20 mV/s.*

root of the transfer curves. The mobility was calculated using Eq. 2.6. Because the measurement speed was very low, the 'DC' value for the capacitance, 19 µF/cm^2, was used. The mobility obtained from both curves was $6 \cdot 10^{-3}$ cm^2/(Vs). It must be noted that there is significant uncertainty in the value of the mobility due to the large leakage current and the hysteresis. The value is much lower than previous results in ion gel gated OTFTs (as high as 1 cm^2/(Vs)), which used P3HT as the semiconductor [19, 53, 54]. This is expected since PTAA is generally a poorer semiconductor. The result does fit in the relatively large range of mobilities obtained for PTAA with other gate dielectrics, from 10^{-5} to 10^{-2} cm^2/(Vs) [22].

The threshold voltage was different in the curves with different drain voltages: +0.03 V for $V_D = -0.5$ V and 0.2 V for $V_D = -1$ V. The origin of this difference is the overall higher current of the transfer curve at $V_D = -1$ V, which may be caused in part by leakage current. The positive threshold voltage implies that the transistor is of 'normally on' type, meaning that it requires a positive gate voltage to turn it off.

The subthreshold slope S obtained from the logarithmic plot of the transfer curves was approximately 0.3 ... 0.4 V/decade. This value is quite large compared with conventional a-Si:H TFTs; a small S indicates that the transistor can function well as a switch. The values of S in previous ion gel gated transistors have been on the order of 0.1 ... 0.2 V/decade, although 0.38 V/decade has been obtained with a gel of similar polymer–ionic liquid combination as in this work [19]. The value of S

obtained here does agree with the results in the literature. The *on-off* ratio is at its best 10^2, which is much lower than in previous work (on the order of 10^5) [19]. This implies that the device does not perform well as a transistor.

When the devices were measured, the color of the semiconductor under the gel was observed to change from light yellow to reddish orange. The color change was not permanent: it faded away when the samples were left undisturbed for days. The reason for the color change is presumably chemical doping of the semiconductor by the ionic liquid or impurities in the gel; the color matched that of intentionally chemically doped PTAA. There may also be some other type of interaction between the PTAA and the ionic liquid. Because the measurement speeds were low, the ions had time to migrate into the semiconductor layer. Slow migration out of the semiconductor, or not completely reversible doping, may also be reasons for the leakage currents between the source and the drain electrodes.

4.2.3 Switching the transistor

The switching properties of the ion gel gated transistor were examined by supplying a square-wave signal of amplitude 2 V to the gate electrode at different frequencies while applying a constant drain voltage. The voltage over the load resistor was measured. The results as well as the measurement circuit are depicted in Fig. 4.7.

Ideally, when the gate voltage is zero (*off* state), the output voltage should be zero as well, because the resistance of the transistor without the channel should be very high compared to the load resistor. The result is that most of the voltage drop between the drain and ground occurs over the transistor channel. In the results of the measurement, this *off* voltage does not go to zero. The reason is likely leakage between the source and the drain: as observed in the output and transfer measurements, the source-drain leakage becomes notable at –1.5 V. Additionally, to completely turn the transistor *off*, a positive gate voltage should be applied, as discussed in the previous section.

In the *on* state, there should ideally be very little resistance between the source and drain electrodes. This means that the output voltage should be the same as the drain voltage. In the results, however, the output has higher negative voltage than the drain voltage. The explanation is that there is a leakage current through the ion gel from the gate (at –2 V) to the source. This increases the overall current through the load resistor, resulting in a more negative value for the output voltage, which is measured over the resistor.

The signal distortion ('spiking') at the beginning of the square waves can be explained by the capacitance produced by the gate-source and gate drain overlap (Fig. 4.7(d)). The current is proportional to the capacitance and the time derivative of the voltage; when the voltage is changed abruptly, its time derivative is very large,

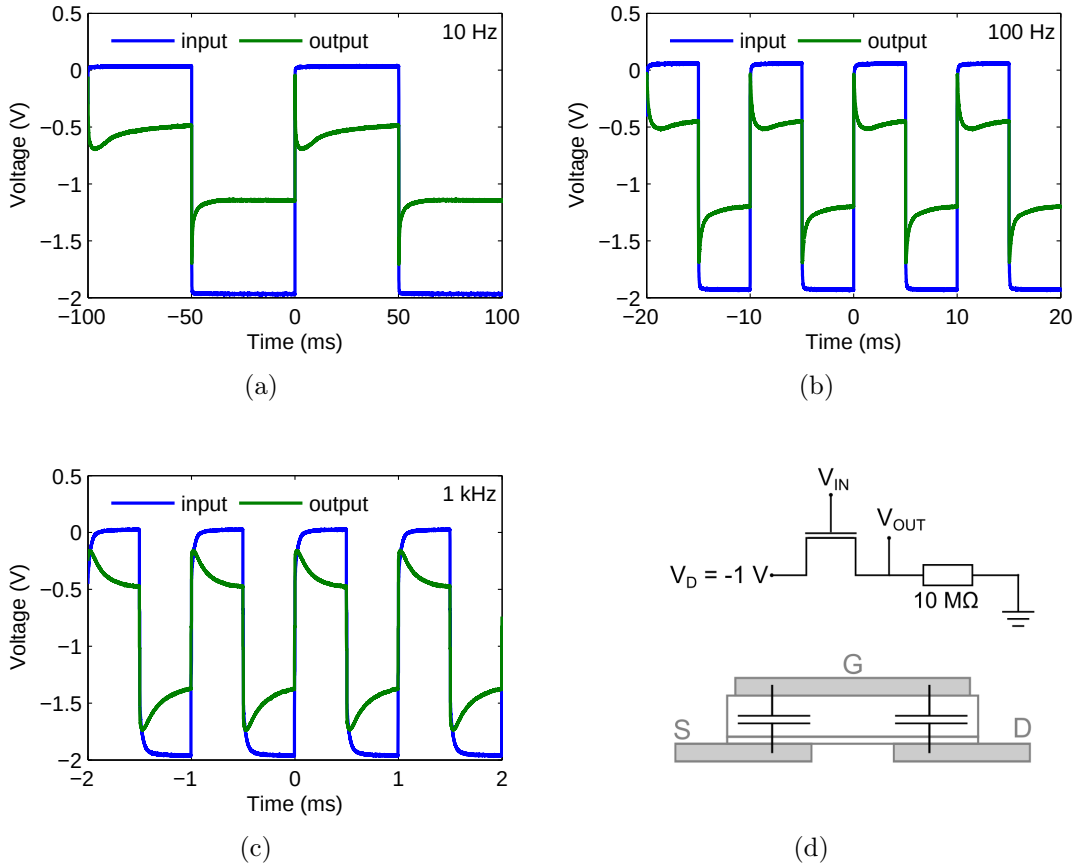

Figure 4.7. *The time response of the ion gel OTFT to a square wave input at the gate electrode at different voltages: (a) 10 Hz, (b) 100 Hz, (c) 1 kHz; (d) shows the measurement circuit diagram and the origin of the capacitance from the gate-source and gate-drain overlap.*

implying a transient current. It is essentially the result of charging and discharging the capacitor. The additional current then increases the voltage observed over the load resistor. This current is most noticeable at the highest frequency, 1 kHz, where the voltage barely has time to even out before switching again.

In the lowest frequency measurement at 10 Hz, there is another effect visible when the transistor is switched *off*: a negative 'bump' appears in the voltage. It is also somewhat visible in the 100 Hz measurement. A possible reason is the combination of the above explained capacitive effect and a slow turning off of the transistor. The latter can be explained as emptying the stored charge in the semiconductor when the gate voltage is turned off. The slow movement of the ions in the gel may slow down the flow of holes further. A similar effect does not occur when the transistor is turned on. The effect is not fast enough to be visible in the 1 kHz measurement.

4.3 Reference OTFT

To compare the ion gel properties with a more conventional dielectric, a reference transistor was fabricated using PMMA as a dielectric. The channel size and gate electrode width were the same as in the ion gel OTFTs to make comparison easy. The only difference was of course that PMMA was spin-coated and the gate electrode was evaporated on top of it. This means the contact between the dielectric and the electrode and semiconductor is somewhat different in the two structures. Spin-coating the dielectric on the semiconductor and evaporating the gold on the dielectric covers the surface despite roughness so there is a good contact to both of them. The ion gel deposition method is different, but the soft, almost liquid nature of the gel should ensure an equally good contact.

4.3.1 Output characteristics of the reference OTFT

The output of the transistors is presented in Fig. 4.8. The most notable characteristics of the reference transistor are the high voltages required for operation as well as the small output currents. Since the channel width and length are identical to that of the ion gel gated OTFT, the currents can be compared directly: the reference OTFT output is three orders of magnitude lower than that of the ion gel OTFT.

The reference device does perform better than the ion gel OTFT in terms of hysteresis and output curve shape. There is however some sublinearity in the output curve at high gate voltage. The origin of this effect is unknown. The current is very small, compared to previous results with PTAA where a saturation current of 200 nA was reached at gate voltage –40 V. In that device the length of the channel

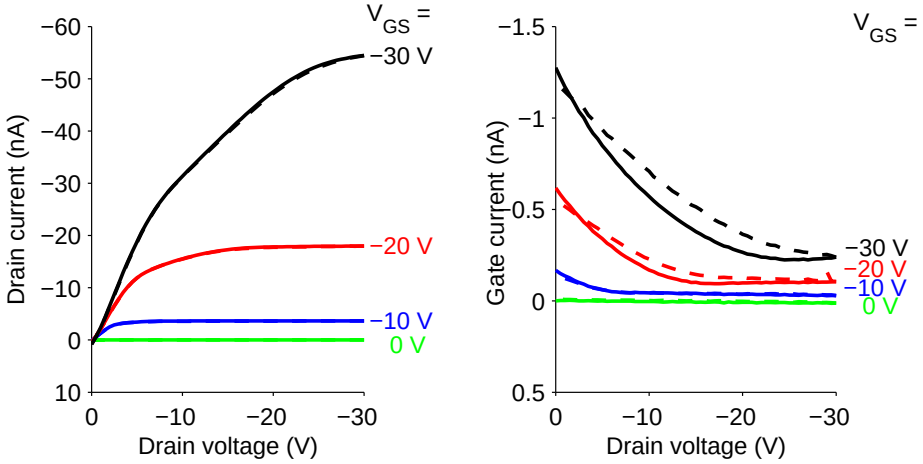

Figure 4.8. *The plot on the left shows the output curves of the reference transistor with different gate voltages and the plot on the right the gate leakage current in the measurement.*

was 30 µm and length 1000 µm, giving the ratio W/L of only 33. The channel current is proportional to W/L (Eq. 2.1). The reference device had W/L of 200, but only produced a slightly more than 50 nA with 30 V gate voltage [28]. It must be noted that not only were the channel dimensions different in these two cases, the dielectric layer was of a different material and thickness, and the PTAA formulation used was not the same one.

4.3.2 Transfer characteristics of the reference OTFT

The transfer properties of the reference OTFTs were examined at different drain voltages and the result from the saturation regime (high drain voltage) measurement is plotted in Fig. 4.9. The capacitance of the PMMA dielectric layer was determined to be approximately 1 nF/cm^2. The on-off ratio is approximately 10^3, which is better than that of the ion gel OTFT. On the other hand, the subthreshold slope is 0.8 V/decade, which is worse than in the ion gel OTFT. This is partly a consequence of the high operating voltage of the reference transistor.

The square root of the transfer curve is also plotted in Fig. 4.9. A straight line was fitted to it, giving a threshold voltage of –3.6 V and mobility $5 \cdot 10^{-4}$ cm^2/(Vs). The mobility is an order of magnitude lower than that determined from ion gels with the same method.

Another approach to determining the mobility was to use the transconductance in the linear region. The transfer curve was measured at a low drain current, yielding a linear dependence between V_G and I_D, which is presented in Fig. 4.10. A straight line was fitted to the plot, and its slope gave the transconductance $g_{m,lin}$. Using Eq. 2.10, the obtained mobility is $5 \cdot 10^{-3}$ cm^2/(Vs), which is an order of magnitude higher than the one determined in the saturation region. It is the same as the

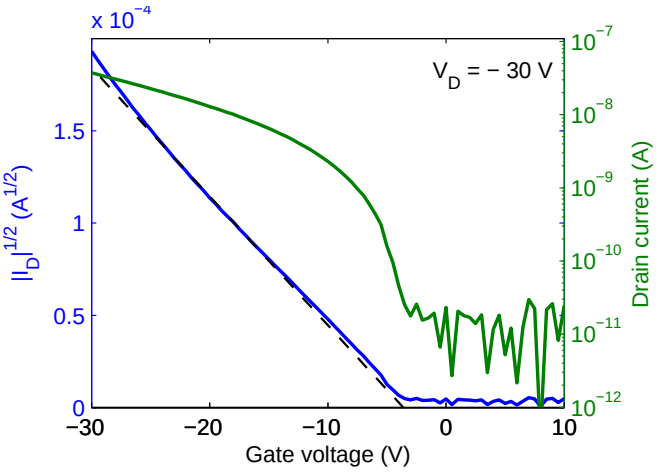

Figure 4.9. *Saturation region transfer curve of the reference OTFT and its square root. The fitted line is shown in black.*

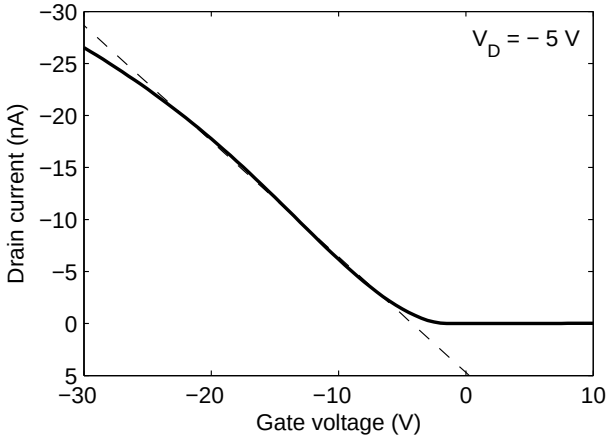

Figure 4.10. *Linear region transfer curve of the reference transistor and the fitted line where the slope is the transconductance,* $g_{m,lin}$.

mobility obtained in the ion gel OTFTs in the saturation region.

There is significant uncertainty in the determination of the mobility in the reference OTFTs. The main reason is that the measurement of the PMMA layer capacitance was done by using the transistor itself, using the overlap area between the drain and gate electrodes. This method ignores the contribution of the semiconductor layer to the capacitance, which may be complicated. The capacitance could have been determined also by preparing a separate sample with just the PMMA between two electrodes, but the spreading of the spin-coated PMMA layer could be drastically different from the one on PTAA, so it was not done. Considering the possible inaccuracy of the ion gel capacitance as well, the only conclusion that can be drawn from the mobility calculations is that there is no significant difference between the mobility in the ion gel and reference transistors. The measured mobility in both is approximately $10^{-3}\,\mathrm{cm}^2/(\mathrm{Vs})$.

5 SUMMARY

The purpose of this thesis was to explore the use of a novel gate dielectric, ion gel, for organic thin-film transistors. The main goal was to fabricate a functioning transistor and to examine its properties. Ion gel gated transistors can be operated at low voltages, i.e. less than 2 V. The low-voltage operation is desirable, because for example printed organic diodes are not compatible with the high voltages usually required by conventional OTFTs. The conventional dielectrics are too thick to allow for large currents to be achieved with low voltages, usually requiring voltages of over 20 V. The electric double layers formed at the ion gel interfaces reduce the effective thickness of the dielectric to Ångström scale, enabling small voltages to be used.

The ion gel used in this work consisted of an ionic liquid and a block copolymer, which form a physically cross-linked gel. The ion gel gated thin film transistor was fabricated using an amorphous semiconductor, PTAA, and gold electrodes. The ionic liquid is corrosive towards electropositive metals such as copper, which prevented the use of a less expensive electrode material. The ion gel was pasted by hand on the semiconductor channel and a gate electrode, evaporated on a separate plastic film, was pressed on top of it. This method of fabrication, though rudimentary, was found to be the only one that functioned with the gel.

Water is a challenge when working with the ion gels, since ionic liquids are very susceptible to absorbing water from ambient air. To minimize water impurities in the gel, solvents were dried and the samples were stored with desiccant. For the measurements, a probe station was built inside a laboratory desiccator. This made it possible to measure the ion gel transistor after keeping it overnight in the desiccator to dry.

The specific capacitance of the ion gel was determined to be approximately $5\,\mu F/cm^2$ at frequencies below 1 MHz. The low-frequency limit as determined from a capacitor discharge measurement was $19\,\mu F/cm^2$. The strong dependence on frequency is characteristic of the electrolytic insulator structure, because the formation of the double layers is limited by the speed of the ions in the gel. To compare with a conventional dielectric, the specific capacitance of a spin-coated PMMA layer was determined to be approximately $1\,nF/cm^2$.

The results from the ion gel transistor, as compared to a reference transistor fabricated with PMMA as dielectric, are promising in terms of voltage and current:

the ion gel transistor produces three orders of magnitude higher output current with less than a tenth of the input voltage of the reference transistor. Hysteresis and gate electrode leakage are, however, problems with the ion gel transistor. Much of the leakage is presumably caused by water impurities in the gel. The hysteresis is due to slow ion movement as well as electrochemical reactions of impurities at the electrodes.

The charge carrier mobilities extracted from the ion gel and reference transistors were on the order of $10^{-3}\,\mathrm{cm}^2/(\mathrm{Vs})$. This was an expected value based on previous reports on PTAA OFETs, although it was somewhat surprising that there was no significant difference between the reference and the ion gel transistor. The higher capacitance of the ion gel was expected to lead to increased trap-filling in the semiconductor, leading to a higher mobility. The subthreshold slope of the reference transistor, 0.8 V/decade, was much poorer than that of the ion gel one, 0.4 V/decade, which was mostly due to the large voltages and small output current of the reference.

The switching properties of the ion gel transistor were examined with a square-wave input measurement. The transistor could switch well up to 1 kHz, but gate leakage and a large overlap capacitance between the gate and the source and drain electrodes interfered with a clean switching behavior. The threshold voltage of the ion gel transistor was positive, indicating that a positive gate voltage is required to deplete enough charge carriers from the semiconductor channel to turn the transistor off. The reason may be the slow movement of the ions in the gel, or an interaction between the ions and the charges in the semiconductor, other than simply electrostatic attraction.

The objective set for this thesis of a functioning OTFT using an ion gel as gate dielectric was achieved. The results are encouraging in that the transistor could be operated at voltages well below 2 V. As this was the first attempt at using ion gels in this laboratory, it was found that the equipment and processing methods available were not enough to ensure sufficiently dry conditions for the handling of the hygroscopic ionic liquid. This affected not only the transistor properties but also resulted in a low yield of functioning devices. Continuing the work with ion gel gated OTFTs would require improving the dry environment conditions in the lab, such as acquiring a sealed 'glove box' inside which a dry atmosphere can be obtained.

Mass production of ion gel OTFTs would demand a more efficient manufacturing method such as printing to be used, and this has been done previously with ion gels. The requirement for dry conditions may complicate mass production ambitions, as a more controlled environment is needed. Another issue is the durability of the finished devices: because of the hygroscopicity, some encapsulation would be required.

REFERENCES

[1] C. K. Chiang, C.R. Fincher Jr, Y.W. Park, A.J. Heeger, H. Shirakawa, E.J. Louis, S.C. Gau, and A.G. MacDiarmid. Electrical conductivity in doped polyacetylene. *Phys. Rev. Lett.*, 39(17):1098–1101, 1977.

[2] A.J. Heeger. Semiconducting and metallic polymers: the fourth generation of polymeric materials (Nobel lecture). *Angew. Chem. Int. Ed*, 40(14):2591–2611, 2001.

[3] J.H. Burroughes, D.D.C. Bradley, A.R. Brown, R.N. Marks, K. Mackay, R.H. Friend, P.L. Burns, and A.B. Holmes. Light-emitting diodes based on conjugated polymers. *Nature*, 347(6293):539–541, 1990.

[4] H. Hoppea and N.S. Sariciftci. Organic solar cells: An overview. *J. Mater. Res*, 19(1924):1945, 2004.

[5] K.E. Lilja, T.G. Bäcklund, D. Lupo, T. Hassinen, and T. Joutsenoja. Gravure printed organic rectifying diodes operating at high frequencies. *Org. Electron.*, 10(5):1011–1014, 2009.

[6] C.Y. Lin, C.H. Tsai, H.T. Lin, L.C. Chang, Y.H. Yeh, Z. Pei, Y.R. Peng, and C.C. Wu. High-frequency polymer diode rectifiers for flexible wireless power-transmission sheets. *Org. Electron.*, 2011.

[7] A. Tsumura, H. Koezuka, and T. Ando. Macromolecular electronic device: Field-effect transistor with a polythiophene thin film. *Appl. Phys. Lett.*, 49(18):1210–1212, 1986.

[8] T.N. Jackson, Y.Y. Lin, D.J. Gundlach, and H. Klauk. Organic thin-film transistors for organic light-emitting flat-panel display backplanes. *IEEE J. Sel. Top. Quant.*, 4(1):100–104, 1998.

[9] C.D. Sheraw, L. Zhou, J.R. Huang, D.J. Gundlach, T.N. Jackson, M.G. Kane, I.G. Hill, M.S. Hammond, J. Campi, B.K. Greening, et al. Organic thin-film transistor-driven polymer-dispersed liquid crystal displays on flexible polymeric substrates. *Appl. Phys. Lett.*, 80(6):1088–1090, 2002.

[10] L. Zhou, A. Wanga, S.C. Wu, J. Sun, S. Park, and T.N. Jackson. All-organic active matrix flexible display. *Appl. Phys. Lett.*, 88:083502, 2006.

[11] E. Cantatore, T.C.T. Geuns, G.H. Gelinck, E. Van Veenendaal, A.F.A. Gruijthuijsen, L. Schrijnemakers, S. Drews, and D.M. De Leeuw. A 13.56-mhz rfid

system based on organic transponders. *IEEE J. Solid-St. Circ.*, 42(1):84–92, 2007.

[12] M.E. Roberts, S.C.B. Mannsfeld, N. Queraltó, C. Reese, J. Locklin, W. Knoll, and Z. Bao. Water-stable organic transistors and their application in chemical and biological sensors. *Proc. Natl. Acad. Sci.*, 105(34):12134, 2008.

[13] T. Sekitani, T. Yokota, U. Zschieschang, H. Klauk, S. Bauer, K. Takeuchi, M. Takamiya, T. Sakurai, and T. Someya. Organic nonvolatile memory transistors for flexible sensor arrays. *Science*, 326(5959):1516, 2009.

[14] Y. Xia, W. Zhang, M. Ha, J.H. Cho, M.J. Renn, C.H. Kim, and C.D. Frisbie. Printed sub-2 V gel-electrolyte-gated polymer transistors and circuits. *Adv. Funct. Mater.*, 20(4):587–594, 2010.

[15] Y.D. Park, Y. Jang, M. Hwang, J.A. Lim, K. Cho, et al. Low-voltage polymer thin-film transistors with a self-assembled monolayer as the gate dielectric. *Appl. Phys. Lett.*, 87:243509, 2005.

[16] CD Dimitrakopoulos, S. Purushothaman, J. Kymissis, A. Callegari, and JM Shaw. Low-voltage organic transistors on plastic comprising high-dielectric constant gate insulators. *Science*, 283(5403):822, 1999.

[17] L. Herlogsson, X. Crispin, N.D. Robinson, M. Sandberg, O.J. Hagel, G. Gustafsson, and M. Berggren. Low-voltage polymer field-effect transistors gated via a proton conductor. *Adv. Mater.*, 19(1):97–101, 2007.

[18] N.J. Kaihovirta, C.J. Wikman, T. Mäkelä, C.E. Wilén, and R. Österbacka. Self-supported ion-conductive membrane-based transistors. *Adv. Mater.*, 21(24):2520–2523, 2009.

[19] J. Lee, L.G. Kaake, J.H. Cho, X.Y. Zhu, T.P. Lodge, and C.D. Frisbie. Ion gel-gated polymer thin-film transistors: Operating mechanism and characterization of gate dielectric capacitance, switching speed, and stability. *J. Phys. Chem. C*, 113(20):8972–8981, 2009.

[20] J. Lee, M.J. Panzer, Y. He, T.P. Lodge, and C.D. Frisbie. Ion gel gated polymer thin-film transistors. *J. Am. Chem. Soc.*, 129(15):4532–4533, 2007.

[21] Arno Kraft. Conducting Polymers. In William Jones, editor, *Org. Mol. Sol.* CRC Press, 1997.

[22] A. Facchetti. Semiconductors for organic transistors. *Mat. Today*, 10(3):28–37, 2007.

[23] Thomas Engel and Philip Reid. *Physical Chemistry*. Benjamin Cummings, San Fransisco, 2006.

[24] Yohai Roichman. Charge transport in conjugated polymers. Research thesis, Israel Institute of Technology, 2004.

[25] Jean-Luc Bredas. The Polyene Series. Center for Materials and Devices for Information Technology Research (CMDITR) Photonics Wiki, 2011. Available at: http://photonicswiki.org/index.php?title=The_Polyene_Series. Accessed 26.9.2011.

[26] Frederik Jakobsson. *Charge transport modulation in organic electronic diodes*. PhD thesis, Norrköping, 2008.

[27] Paul A. Tipler and Ralph A. Llewellyn. *Modern Physics*. Pearson Prentice Hall, San Fransisco, 2006.

[28] I. McCulloch and M. Heeney. Polytriarylamine semiconductors. *Mat. Matt.*, 4(3):70–71, 2009.

[29] M.E. Galvin. Electrically active polymers and their application. *J. Miner. Met. Mater. Soc.*, 49(3):52–55, 1997.

[30] Y. Shirota and H. Kageyama. Charge carrier transporting molecular materials and their applications in devices. *Chem. Rev.*, 107(4):953–1010, 2007.

[31] G. Malliaras and R. Friend. An organic electronics primer. *Phys. Today*, 58:53, 2005.

[32] Demetrio A. da Silva Filho, Yoann Olivier, Veaceslav Coropceanu, Jean-Luc Brédas, and Jérôme Cornil. Theoretical Aspects of Charge Transport in Organic Semiconductors: A Molecular Perspective. In Zhenan Bao and Jason Locklin, editors, *Organic Field-Effect Transistors*. CRC Press, 2007.

[33] Ben G. Streetman and Sanjay Kumar Banerjee. *Solid State Electronic Devices*. Pearson Prentice Hall, San Fransisco, 2006.

[34] H. Sirringhaus. Device physics of solution-processed organic field-effect transistors. *Adv. Mat.*, 17(20):2411–2425, 2005.

[35] V. Coropceanu, J. Cornil, D.A. da Silva Filho, Y. Olivier, R. Silbey, and J.L. Brédas. Charge transport in organic semiconductors. *Chem. Rev.*, 107(4):926–952, 2007.

[36] R.A. Marcus. Electron transfer reactions in chemistry. theory and experiment. *Rev. Mod. Phys.*, 65(3):599, 1993.

[37] S.V. Novikov, D.H. Dunlap, V.M. Kenkre, P.E. Parris, and A.V. Vannikov. Essential role of correlations in governing charge transport in disordered organic materials. *Phys. Rev. Lett.*, 81(20):4472–4475, 1998.

[38] S. Schols, S. Verlaak, C. Rolin, D. Cheyns, J. Genoe, and P. Heremans. An organic light-emitting diode with field-effect electron transport. *Adv. Funct. Mater.*, 18(1):136–144, 2008.

[39] Electron work function of the elements. In W.M. Haynes, editor, *CRC Handbook of Chemistry and Physics*. CRC Press/Taylor and Francis, Boca Raton, FL, 92nd edition, 2012. (Internet Version 2012).

[40] G. Horowitz. Organic field-effect transistors. *Adv. Mat.*, 10(5):365–377, 1998.

[41] S. M. Sze. *Physics of Semiconductor Devices*. John Wiley & Sons, 1981.

[42] Michael Shur. *Physics of Semiconductor Devices*. Prentice-Hall International, Englewood Cliffs, N.J., 1990.

[43] Jean-Pierre Colinge and Cynthia A. Colinge. *Physics of Semiconductor Devices*. Kluwer Academic Publishers, 2002.

[44] H. P. Myers. *Introductory Solid State Physics*. Taylor & Francis, 2nd edition, 1997.

[45] D. Braga and G. Horowitz. High-performance organic field-effect transistors. *Adv. Mat.*, 21(14-15):1473–1486, 2009.

[46] Tomas Bäcklund. *Hygroscopic Insulator Organic Transistor: Solution Processing, Low-Voltage Performance, and Chemical Effects*. PhD thesis, Åbo Akademi University, 2005.

[47] J. Veres, S. Ogier, G. Lloyd, and D. de Leeuw. Gate insulators in organic field-effect transistors. *Chem. Mater.*, 16(23):4543–4555, 2004.

[48] L.L. Chua, P.K.H. Ho, H. Sirringhaus, and R.H. Friend. High-stability ultrathin spin-on benzocyclobutene gate dielectric for polymer field-effect transistors. *Appl. Phys. Lett.*, 84:3400, 2004.

[49] G.T. Barnes and I.R. Gentle. *Interfacial Science*. Oxford University Press, 2005.

[50] J. Veres, S.D. Ogier, S.W. Leeming, D.C. Cupertino, and S. Mohialdin Khaffaf. Low-k insulators as the choice of dielectrics in organic field-effect transistors. *Adv. Funct. Mat.*, 13(3):199–204, 2003.

[51] M.L. Chabinyc and A. Salleo. Materials requirements and fabrication of active matrix arrays of organic thin-film transistors for displays. *Chem. Mater.*, 16(23):4509–4521, 2004.

[52] M.J. Panzer and C.D. Frisbie. Polymer electrolyte-gated organic field-effect transistors: Low-voltage, high-current switches for organic electronics and testbeds for probing electrical transport at high charge carrier density. *J. Am. Chem. Soc.*, 129(20):6599–6607, 2007.

[53] J.H. Cho, J. Lee, Y. He, B.S. Kim, T.P. Lodge, and C.D. Frisbie. High-capacitance ion gel gate dielectrics with faster polarization response times for organic thin film transistors. *Adv. Mater.*, 20(4):686–690, 2008.

[54] J.H. Cho, J. Lee, Y. Xia, B.S. Kim, Y. He, M.J. Renn, T.P. Lodge, and C.D. Frisbie. Printable ion-gel gate dielectrics for low-voltage polymer thin-film transistors on plastic. *Nat. Mater.*, 7(11):900–906, 2008.

[55] Z. Bao, A. Dodabalapur, and A.J. Lovinger. Soluble and processable regioregular poly (3-hexylthiophene) for thin film field-effect transistor applications with high mobility. *Appl. Phys. Lett.*, 69:4108, 1996.

[56] Z. Bao, Y. Feng, A. Dodabalapur, VR Raju, and A.J. Lovinger. High-performance plastic transistors fabricated by printing techniques. *Chem. Mater.*, 9(6):1299–1301, 1997.

[57] I. Krossing, J.M. Slattery, C. Daguenet, P.J. Dyson, A. Oleinikova, and H. Weingärtner. Why are ionic liquids liquid? a simple explanation based on lattice and solvation energies. *J. Am. Chem. Soc.*, 128(41):13427–13434, 2006.

[58] M.J. Earle and K.R. Seddon. Ionic liquids. green solvents for the future. *Pure Appl. Chem.*, 72(7):1391–1398, 2000.

[59] T. Ueki and M. Watanabe. Macromolecules in ionic liquids: Progress, challenges, and opportunities. *Macromolecules*, 41(11):3739–3749, 2008.

[60] R.P. Swatloski, S.K. Spear, J.D. Holbrey, and R.D. Rogers. Dissolution of cellulose with ionic liquids. *J. Am. Chem. Soc.*, 124(18):4974–4975, 2002.

[61] P. Wang, S.M. Zakeeruddin, J.E. Moser, and M. Grätzel. A new ionic liquid electrolyte enhances the conversion efficiency of dye-sensitized solar cells. *J. Phys. Chem. B*, 107(48):13280–13285, 2003.

[62] A. Lewandowski and A. Swiderska-Mocek. Cheminform abstract: Ionic liquids as electrolytes for li-ion batteries: An overview of electrochemical studies. *ChemInform*, 41(38), 2010.

[63] D.R. MacFarlane, M. Forsyth, P.C. Howlett, J.M. Pringle, J. Sun, G. Annat, W. Neil, and E.I. Izgorodina. Ionic liquids in electrochemical devices and processes: managing interfacial electrochemistry. *Accounts Chem. Res.*, 40(11):1165–1173, 2007.

[64] U. Domańska. General review of ionic liquids and their properties. In M. Koel, editor, *Ionic Liquids in Chemical Analysis*. Taylor & Francis, 2005.

[65] P. Walden. Molecular weights and electrical conductivity of several fused salts. *Bull. Acad. Imper. Sci.(St. Petersburg)*, 1800:405–422, 1914.

[66] J.S. Wilkes, J.A. Levisky, R.A. Wilson, and C.L. Hussey. Dialkylimidazolium chloroaluminate melts: a new class of room-temperature ionic liquids for electrochemistry, spectroscopy and synthesis. *Inorg. Chem.*, 21(3):1263–1264, 1982.

[67] Jonathan Clayden, Nick Greeves, Stuart Warren, and Peter Wothers. *Organic Chemistry*. Oxford University Press, 2001.

[68] Leslie Howard Sperling. *Introduction to Physical Polymer Science*. Wiley, Hoboken, NJ, USA, 4th edition, 2005.

[69] JY Song, YY Wang, and CC Wan. Review of gel-type polymer electrolytes for lithium-ion batteries. *J. Power Sources*, 77(2):183–197, 1999.

[70] Y. Osada. Electrical behaviors and mechanical Responses of Polyelectrolyte Gels. In Y. Osada and Khokhlov A. R., editors, *Polymer Gels and Networks*. CRC Press, 2001.

[71] M.A.B.H. Susan, T. Kaneko, A. Noda, and M. Watanabe. Ion gels prepared by in situ radical polymerization of vinyl monomers in an ionic liquid and their characterization as polymer electrolytes. *J. Am. Chem. Soc.*, 127(13):4976–4983, 2005.

[72] T.P. Lodge. A Unique Platform for Materials Design. *Science*, 321(5885):50, 2008.

[73] Y. He, P.G. Boswell, P. Bühlmann, and T.P. Lodge. Ion gels by self-assembly of a triblock copolymer in an ionic liquid. *J. Phys. Chem. B*, 111(18):4645–4652, 2007.

[74] M. Galinski, A. Lewandowski, and I. Stepniak. Ionic liquids as electrolytes. *Electrochim. Acta*, 51(26):5567–5580, 2006.

[75] P. Bonhote, A. P. Dias, N. Papageorgiou, K. Kalyanasundaram, and M. Grätzel. Hydrophobic, highly conductive ambient-temperature molten salts. *Inorg. Chem.*, 35(5):1168–1178, 1996.

[76] J. Zhang, W. Wu, T. Jiang, H. Gao, Z. Liu, J. He, and B. Han. Conductivities and viscosities of the ionic liquid [bmim][pf6]+ water+ ethanol and [bmim][pf6]+ water+ acetone ternary mixtures. *J. Chem. Eng. Data*, 48(5):1315–1317, 2003.

[77] J.A. Widegren, E.M. Saurer, K.N. Marsh, and J.W. Magee. Electrolytic conductivity of four imidazolium-based room-temperature ionic liquids and the effect of a water impurity. *J. Chem. Thermodyn.*, 37(6):569–575, 2005.

[78] K.R. Seddon, A. Stark, M.J. Torres, et al. Influence of chloride, water, and organic solvents on the physical properties of ionic liquids. *Pure Appl. Chem*, 72(12):2275–2287, 2000.

[79] J. N. A. Canongia Lopes and A. A. H. Pádua. Nanostructural organization in ionic liquids. *J. Phys. Chem. B*, 110(7):3330–3335, 2006.

[80] J.R. Miller and P. Simon. Fundamentals of electrochemical capacitor design and operation. *Elec. Soc. Interface*, 17(1):31–32, 2008.

[81] P. Simon and Y. Gogotsi. Materials for electrochemical capacitors. *Nat. Mat.*, 7(11):845–854, 2008.

[82] M. Ishikawa, M. Ihara, M. Morita, and Y. Matsuda. Electric double layer capacitors with new gel electrolytes. *Electrochim. acta*, 40(13-14):2217–2222, 1995.

[83] F. Endres and S.Z. El Abedin. Air and water stable ionic liquids in physical chemistry. *Phys. Chem. Chem. Phys.*, 8(18):2101–2116, 2006.

[84] M. Ha, Y. Xia, A.A. Green, W. Zhang, M.J. Renn, C.H. Kim, M.C. Hersam, and C.D. Frisbie. Printed, sub-3v digital circuits on plastic from aqueous carbon nanotube inks. *ACS Nano*, 2010.

[85] B.J. Kim, H. Jang, S.K. Lee, B.H. Hong, J.H. Ahn, and J.H. Cho. High-performance flexible graphene field effect transistors with ion gel gate dielectrics. *Nano Lett.*, 2010.

[86] B.S. Ong, Y. Wu, P. Liu, and S. Gardner. High-performance semiconducting polythiophenes for organic thin-film transistors. *J. Am. Chem. Soc.*, 126(11):3378–3379, 2004.

[87] IEEE Standard 1680-2008: IEEE Standard for Test Methods for the Characterization of Organic Transistors and Materials, 2008.